BIOPRINTING OF THREE-DIMENSIONAL MODELS TO EVALUATE ADIPOCYTE BREAST CANCER CELL INTERACTIONS AND MIGRATION

By

SARAH MARIE CHAJI

(Under the Direction of Cheryl Gomillion)

ABSTRACT

There is an increasing demand for the development of novel breast cancer cell and tissue models mimicking the breast microenvironment to develop breast cancer treatments. These new models could be used for research applications, such as evaluating tumor cell behavior and screening of therapeutics. Currently, widely used two-dimensional (2D) models are limited due to a lack of appropriate chemical cues and physiological architecture of the complex breast microenvironment. Thus, three-dimensional (3D) *in vitro* models have been increasingly investigated for improved cell and disease modeling platforms. At present, 3D bioprinting has emerged as a popular method for fabricating 3D tissue structures. However, the primary obstacles with 3D bioprinting are cost and size of some printers. In this work, the feasibility for efficiently and economically fabricating 3D bioprinted models for the purpose of evaluating the breast tumor microenvironment, including studying the relationship between adipocytes and cancer cells has been established.

INDEX WORDS: breast cancer, 3D bioprinting, hydrogel, breast cancer metastasis, bioink, tumor spheroids, adipocytes

BIOPRINTING OF THREE-DIMENSIONAL MODELS TO EVALUATE ADIPOCYTE BREAST CANCER CELL INTERACTIONS AND MIGRATION

By

SARAH MARIE CHAJI

B.S. Biological Engineering, University of Georgia, 2017

A Thesis Submitted to the Graduate Faculty of the University of Georgia in Partial Fulfillment of the Requirements for the Degree

MASTERS OF SCIENCE

ATHENS, GEORGIA

2019

©2019

Sarah Marie Chaji

All Rights Reserved

BIOPRINTING OF THREE-DIMENSIONAL MODELS TO EVALUATE ADIPOCYTE BREAST CANCER CELL INTERACTIONS AND MIGRATION

By

SARAH MARIE CHAJI

Major Professor: Cheryl Gomillion

Committee Members: Rodney Averett

Ramana Pidaparti

Electronic Version Approved:

Suzanne Barbour
Dean of the Graduate School
The University of Georgia
August 2019

DEDICATION

I would like to dedicate this work to:

My parents, Zach Chaji and Maria Camara, for all of their continuous love and support.

My sister, Marina Chaji, for always being supportive, keeping me sane, and guiding me in the right direction.

ACKNOWLEDGEMENTS

I would like to acknowledge:

My principal investigator, mentor, and friend, Dr. Cheryl Gomillion. Thank you for all of your tremendous about of help throughout the years and for your never ending supply of patience. I could not have found a better advisor or a better lab.

My lab mates and friends for continuously pushing me to succeed.

Dr. Rodney Averett and Dr. Ramana Pidaparti for their service on my committee.

TABLE OF CONTENTS

LIST OF FIGURES

Chapter 2

Chapter 3

Chapter 4

LIST OF TABLES

CHAPTER 1

INTRODUCTION

In today's society the word cancer is ubiquitous. With more than 100 different types of cancer and approximately 18.1 million new cancer cases globally each year, cancer seems to be unavoidable [1]. More specifically, those diagnosed with lung cancer or breast cancer have an 18.4% and 11.6% likelihood of cancer-related mortality, respectively [1]. Year after year, breast cancer continuous to pave the way as the second leading cause of cancer death [1-3], where approximately 1 in every 8 women will be diagnosed with this disease and an estimated 40,610 breast cancer deaths will occur annually in the United States (U.S.) alone [2, 3]. Thus making breast cancer the second most commonly diagnosed form of cancer in women in the U.S., accounting for 1 in every 3 cancers diagnosed [2]. Breast cancer tumor size, nodal involvement, and invasiveness is divided into stages. Stage IV breast cancer, also referred to as metastatic breast cancer, is known to be the most deadly due to its ability to quickly grow and spread to other organs and the lymphatic system [4]. Of those diagnosed with breast cancer, it is estimated that approximately 20 - 25% will have a form of triple-negative breast cancer [5, 6]. Triple-negative breast cancers, as demonstrated with MDA-MB-231 and HCC1806 cell lines commonly used for research purposes, are metastatic with a 22% five-year survival rate [6-8].

While breast cancer seems to be threatening enough, there are additional genetic and environmental factors that could stimulate and worsen the aggressiveness of breast

cancer [9]. A main contributor that may increase the risk of breast cancer in post-menopausal women is obesity. Secretory factors from large amounts of adipocytes located in fat deposits of obese patients drive the production of breast cancer [10, 11]. These secretions have the ability to cause a faster tumor growth rate, a decrease in vascularization within the tumor, and an increase in hypoxic areas [10]. Once stimulation of these breast cancer cells occurs, they promote a feedback mechanism that excites the conversion of adipocytes to cancer-associated adipocytes [11, 12]. These new altered cells cyclically feed off of one another, creating a serious alteration to normal cellular processes [11, 12].

Breast cancer has been thought to have been around since 2500 BC, yet there is still no cure [13]. Current treatments for this disease can be partitioned into local treatments and systemic treatments [14]. Local treatments are methods that target the tumor without involving the rest of the body. Local treatments include radiation or surgeries, such as a lumpectomy or a mastectomy [14]. Systemic treatments, on the other hand, are a form of drug that can reach cancer cells anywhere within the body via oral depository or injection [14]. Systemic treatments include chemotherapy, hormone therapy, targeted therapy, and immunotherapy. Yet even with these treatments, success of breast cancer treatments and patient survival rates have known to differ between patients of different ethnicities [14].

With there being no common gold standard for current breast cancer treatments and a lack of a definitive cure, there is great motivation to find new ways to study and ultimately cure this disease. For decades, researchers have modeled breast cancer in a two-dimensional (2D) platform (i.e., monolayer cell cultures), which lacks the appropriate

chemical cues and physiological architecture of breast cancer *in vivo* [15, 16]. The push towards developing alternative modeling approaches has unveiled the possibility of three-dimensional (3D) modeling of the breast cancer tumor environment. While multiple fabrication methods for 3D models have been investigated, 3D bioprinting, specifically, has the ability to rapidly recreate the complex 3D microenvironments [17, 18] concurrently, while having the potential to use biocompatible bioinks to achieve tunable desired shapes and mechanical properties [17]. Nevertheless, the largest caveat with 3D bioprinting is the cost and size of most printers. Existing 3D bioprinters tend to be large and can cost from $10,000 to over $200,000 [19]. Typically, those with limited space and funds would not have access to this advanced fabrication tool.

Therefore, the overarching goal of this work was to demonstrate the feasibility of 3D bioprinting and its use as a tool for studying the breast cancer environment via an affordable platform. The more specific objective of this work was to explore the possibility of high-throughput screening of breast cancer through the production of cell-specific breast cancer tumor environments. This was done by proving the feasibility of 3D bioprinting the breast cancer microenvironment by converting a small low-cost 3D extrusion printer into an affordable 3D bioprinter, evaluating comparable bioink properties, testing cell viability and adipogenic potential, and studying the migration of metastatic breast cancer cells and their secretomes. Chapter 2 of this thesis will deliver background knowledge and an overview of breast cancer, 3D models, and bioinks. Chapter 3 will then detail proof-of-concept testing to show the functionality of the optimized bioprinter to recreate the 3D breast cancer tumor environment in the form of tumor spheroids. In Chapter 4, a study of adipocyte-breast cancer cell interactions will be presented, with

analysis of cell secreted biomolecules and assessment of breast cancer migration ability through multiple 3D techniques. Lastly, Chapter 5 will provide a summary of overall findings and present finals thoughts and proposed suggestions for future work.

CHAPTER 2

LITERATURE REVIEW

2.1 BREAST ANATOMY AND PHYSIOLOGY

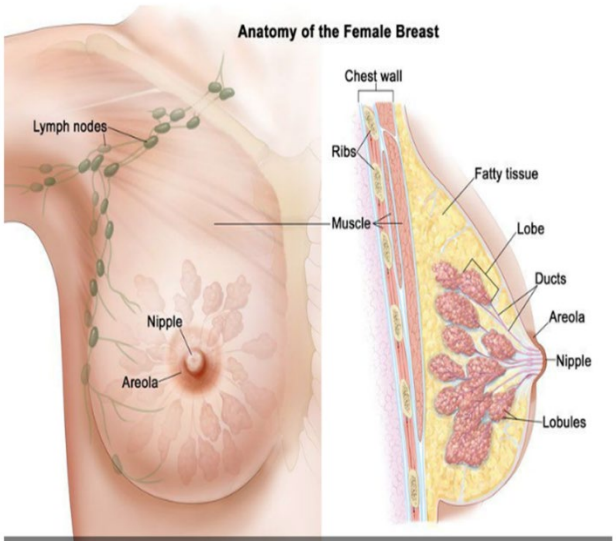

Figure 2.1. The breast anatomy [20].

The breast, located at the anterior of the chest, is referred to as the area of tissue that holds the mammary glands. The primary tissue types within the breast include adipose tissue and glandular tissue [21]. The main function of the breast is to produce milk through these mammary glands during lactation. As shown in Figure 2.1, the female breast is comprised mostly of the chest wall, fatty tissue, lobes, lobules, and ducts. Each breast consists of roughly 15-20 lobes that hold lobules [21]. The lobules produce milk through lactogenesis, where the milk travels through the ducts and exits out the nipple.

The initiation of lactogenesis is based on hormone regulation. Lactogenesis I begins at approximately 15-20 weeks of pregnancy when high levels of progesterone inhibit the production of milk. Lactogensis II occurs after childbirth when prolactin levels remain high and the estrogen, progesterone, and human placental lactogen levels suddenly drop, stimulating the production of milk. While Lactogenesis I and II are hormone-driven, the final stage of lactogenesis is not. Lactogenesis III works based on the ongoing milk production called galactopoiesis, making it driven by milk removal [22, 23]. As shown in Table 2.1, hormones play a crucial role in the breast environment. The constant fluctuation of hormone levels not only affects lactation product, but causes modifications to other cells in the breast. One serious threat from these fluctuations is the stimulation of breast cancer that could result [24].

Table 2.1. Hormones involved in lactation [22].

Hormone	Response
Prolactin	Growth: nipple and areola
Human placental lactogen	
Estrogen	Proliferation and differentiation: ducts and glandular system
Progesterone	Growth: lobes, lobules, alveoli
	Inhibition of lactation and milk secretion
Decrease of estrogen and progesterone (placenta removal)	Prolactin uninhibited
Increase of prolactin	Milk synthesis
Oxytocin (milk suckling)	Milk ejection reflex (MER)
	Myoepithelial cell contraction

Throughout the pubescent years, glandular tissue begins to form and increases in density. The glandular tissue is what alters the lactation function within the breast. The vast amount of excess tissue within the breast consists of fatty (i.e., adipose) tissue, which supports and protects the lobes and ducts. Adipose tissue begins around the collar bone and extends to roughly halfway down the rib cage. The adipose tissue portion of the breast also holds a network of nerves, lymph vessels, ligaments, blood vessels, and fibrous connective tissue. The breast increases in size as the lipids within the adipose tissue increases. The size, density, and shape of women's breasts largely vary based on factors such as genetics, diet, and environment [25]. The breast will only obtain full maturity during pregnancy when the hormone prolactin stimulates the production of

lactate and swelling of the lobules and lobes. The regulation of estrogen and progesterone hormones within the body prevents lactation prior to the arrival of the baby [26]. On the other hand, at the onset of menopause, the breast begins to atrophy due to reduced levels of estrogen and progesterone [27], thus, hormone fluctuation plays a large role in the breast tissue environment.

2.2 BREAST CANCER FORMATION AND TUMOR PROGRESSION

Breast cancer is formed from rapid uncontrolled division and replication of mutated cells in the breast. This mutation is cause by an error in the DNA sequence. The tumor forms when the genetically altered cell begins proliferating when it should not, referred to as hyperplasia (Figure 2.2). Another frequent occurrence is dysplasia where the cells resulting from abundant proliferation can typically appear abnormal in shape and orientation [28]. At this stage, the tumor formed can be either invasive or non-invasive. Benign, non-invasive, tumors are not considered to be cancerous and tend to remain in the lobes or ducts [29, 30].

Figure 2.2. Breast tumor development [28].

Invasive or malignant tumors, however, are cancerous and invade other healthy cells in the body. Breast cancer typically forms in the lobes where milk is produced or in

the ducts where milk is transported [29]. Breast cancer that begins in the lobes is called lobular carcinoma *in situ* (LCIS) and can be non-invasive or can spread throughout the ducts. Ductal carcinoma *in situ* (DCIS) is cancer that forms in the ducts, which can also be non-invasive or can spread to common areas like the bone, blood, liver, or brain [29]. Lastly, there is stromal tissue carcinoma, which is less prevalent, but occurs in the fatty fibrous tissue of the breast. This spread, or metastasis, of cancerous cells is due to small cells breaking off from the tumor and migrating to other parts of the body [5]. Risk factors that can lead to these mutations include, but are not limited to, genetics, excessive alcohol consumption, obesity, use of oral contraceptives, late menopause, radiation, and diet [30]. The specific oncogenesis gene for the receptor of epidermal growth factor in breast cancer is erb-B or erb-B2 also referred to as HER2. The gene for proteins involved in stopping the cell cycle for breast cancer is RB, BRCA1, and the BRCA2 gene [28].

The three main receptors concerning breast cancer include estrogen receptor (ER), progesterone receptor (PR), and human epidermal growth factor receptor type 2 (HER2). Triple-negative breast tumors (ER-/PR-/HER-) lack all three of these main receptors [31], which results in greater difficulty treating this type of cancer with commonly available therapeutics. This form of breast cancer is commonly found in African-American, Hispanic, or younger women [32, 33]. Cell lines commonly used for studying triple-negative breast cancer include MDA-MB-231 cells derived from a Caucasian donor, while the HCC1806 cells are derived from an African-American donor, presenting cell populations that could be used to study potential differences between patients of different ethnicities. Triple-negative breast cancer is known to be metastatic making it more aggressive [5, 34, 35]. Metastatic breast cancer (MBC) is known to grow and spread more

rapidly than other types of cancer making it more difficult to treat [33]. MBC, frequently referred to as Stage IV breast cancer, will likely migrate to other areas of the body including the bone, blood, liver, and brain. Patients with MBC have a reported five-year survival rate of up to 27% [36]. The lymph vessels and lymph nodes work as the lymph system by transmitting disease-fighting cells and fluids across the body. The lymph nodes remove abnormal cells away from healthy tissue. While the lymphatic system can be useful for the removal of abnormal cells, it is also the primary location for the spread of metastatic breast cancer [36]. The growth of lymphatic vessels, lymphangiogenesis, is activated by cancer and inflammation. Researchers were able to observe a correlation between the metastatic tumor dispersion and the density and growth of the lymphatic vessels [37]. The tumor cells can work by using chemokine attractants that lead them to the lymphatic vessels by entering openings in the endothelial cell junctions or by inducing their own spacing in the endothelial cell layer [37]. Once inside the lymphatic vessels, the breast cancer cells can now migrate throughout the body.

Current treatments for breast cancer can be either local or systematic. Local treatments include surgery and radiation, while systemic treatments include chemotherapy, hormone therapy, targeted therapy, and immunotherapy. While there are various treatment options for breast cancer, there is still no cure [38]. Even though MBC is more aggressive and invasive, the same treatment methods used for normal breast cancer are used, however, their efficacy for treating MBC are limited. Those with metastatic breast cancer are typically treated by systemic therapies because the cancer has spread beyond just the breast tissue and neighboring lymph nodes. While these treatments can slow the growth of the tumor and improve the symptoms, this type of

breast cancer is considered incurable [38]. In addition, many of the current treatments on the market much like Herceptin and Perjeta target specific receptors such as the estrogen receptor (ER), progesterone receptor (PR), or human epidermal growth factor receptor 2 (HER2) [38]. However, metastatic breast cancers that are triple negative lack these receptors. With no innovative techniques for treating MBC, this form of breast cancer is less likely to be treated.

2.3 BREAST CANCER AND ADIPOCYTES

Adipose tissue plays a significant role in breast cancer and breast cancer metastasis [39]. Adipose tissue within the breast is comprised primarily of fibroblasts, macrophages, and adipocytes. Adipocytes are the cells responsible for the storage of fat, which can be found in connective tissue [40]. These adipocytes can provide energy to breast cancer cells in the form of triglycerides, in addition to creating a feedback loop that stems from the secretion of cytokines and hormones, as shown in Figure 2.3 [41].

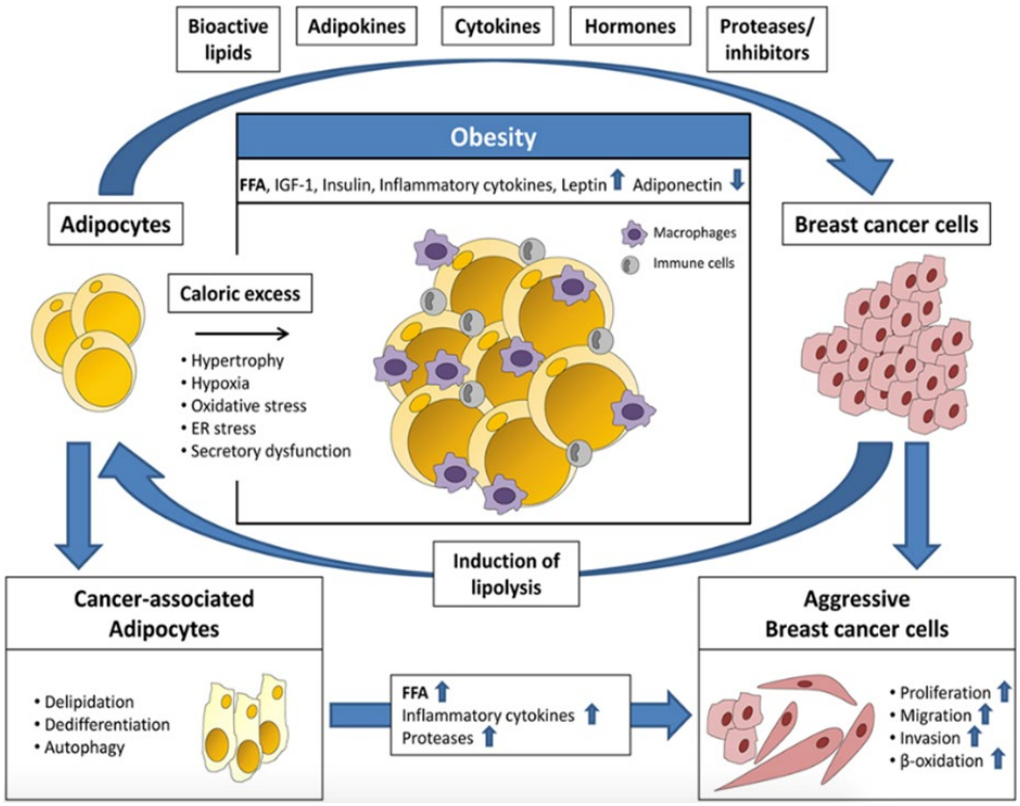

Figure 2.3. Adipocytes and breast cancer cell cycle [12].

These adipocytes secrete factors, including hormones, fatty acids, cytokines, bioactive lipids, and adipokines that affect breast cancer behavior with respect to tumor growth and survival [42]. For example, breast cancer has been linked to body mass index (BMI) due to the influence of adipocytes and their secretomes. Co-culturing adipocytes with cancer cells has demonstrated upregulation of osteopontin, tumor necrosis factor-alpha (TNFα), interleukin-6 (IL-6), IL-1B, leptin, and adiponectin [43], while adipocytes alone are known to secrete factors such as TNFα, adiponectin, IL-6, and leptin. The addition of adipocytes to cancer cells and vice versa promotes a change in secretion rate otherwise viewed as insignificant if the cells were in a monoculture. Further, adipocytes can specifically act as an estrogen signal for breast cancer cells [41, 44]. Postmenopausal

women have increased levels of estradiol and estrone ultimately increasing their BMI. This increased BMI is then correlated to the increased estrogen levels as the adipocytes act as an estrogen signal. When the estrogen signal is being increased in postmenopausal women, there is a higher risk of breast cancer [27, 44-46]. These factors upregulate the production of breast cancer cells, thus making a more aggressive breast cancer cell type. The aggressive breast cancer cells secrete their own inflammatory cytokines and proteases, which aid in the production of cancer-associated adipocytes, continuing a very deadly cycle [41]. Research has demonstrated a link between BMI and breast cancer [47-49]. In addition, it is believed that for postmenopausal women, those who are also overweight are 1.5 times more likely to develop breast cancer and those who are obese are 2 times more likely [50], thus affirming the relationship between adipocytes and breast cancer as one that should be studied further when considering development of therapeutics, etc.

2.4 THREE-DIMENSIONAL (3D) BREAST CANCER MODEL SYSTEMS

Two-dimensional (2D) modeling, usually performed in a monolayer platform, has been used as the gold standard for *in vitro* cultures for decades [51, 52]. 2D models are advantageous because they are affordable and simple. This type of modeling is conducted by growing cells on a rigid platform typically made of polystyrene or glass. These platforms include flasks, plates, and slides [51, 52]. Culturing cells in 2D is easier than doing so in a three-dimensional (3D) platform. Since this modeling technique has been around since the early 1900s and became well-established in the 1940s, there is an abundance of comparative literature, as 2D culture is the most widely used and accepted

amongst researchers and being able to compare experimental results to successful trials from other scientists is a staple in cell culture research [51-53]. However, while conventional 2D modeling has long been marked as the standard for *in vitro* testing, these cultures are unable to replicate the characteristics of human physiology as can be seen in Figure 2.4. In particular, 2D platforms lack the appropriate chemical cues and physiological architecture present in the human body [51-53].

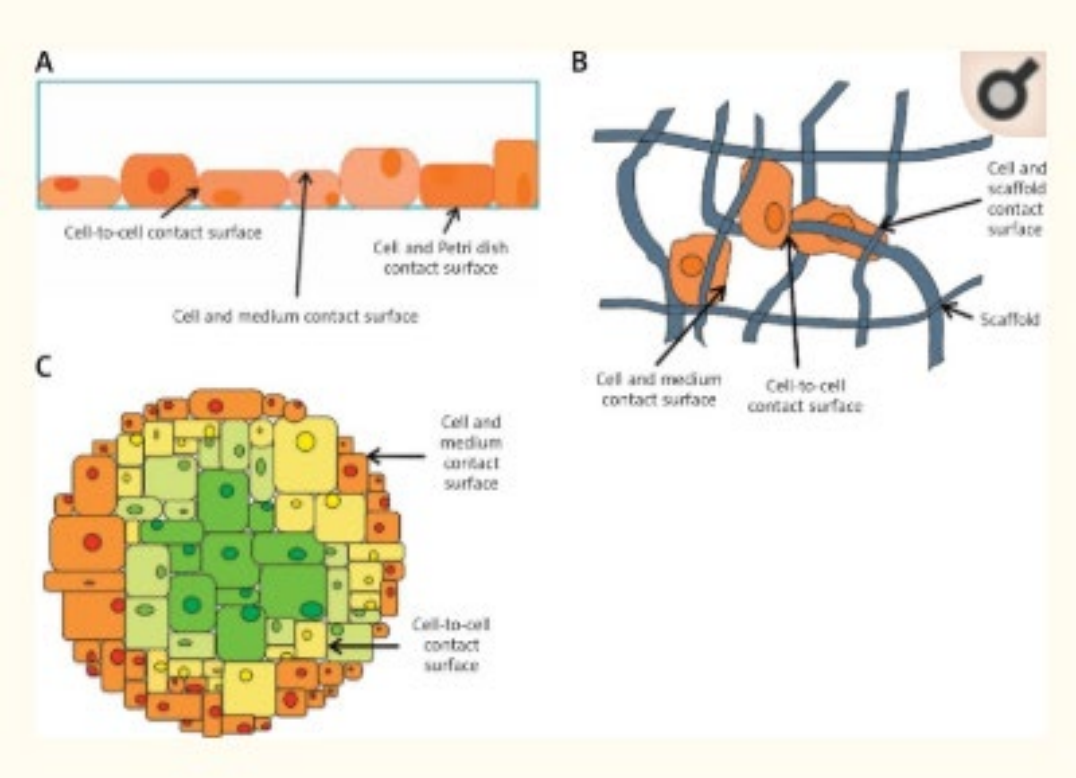

Figure 2.4. Commonly used 2D and 3D cell culture models [52]

The use of 3D models has allowed for a better understanding of cellular differentiation, homeostasis, and tissue organization of the breast cancer environment [16], particularly because studying of cell-cell and cell-extracellular matrix interactions is

easier in 3D platforms [51]. Many researchers are currently using 3D modeling of various cancers, including breast cancer, to study the role of adhesion molecules in metastasis, angiogenesis, and apoptosis [54-56]. Studies of this kind are commonly performed in animal models, however the use of 3D models allows for better control for the differences that may exist among animal species because of reduced variability. 3D modeling has become the ideal method for bridging the gap between 2D culturing and animal models, where we can now observe cellular interactions without the concern for harming an animal during *in vivo* studies [16].

The need for 3D models further stems from the heterogeneity of tumors and from the current resistance of certain tumors to chemotherapy. The tumor microenvironment is comprised of a variety of different cell types, including non-cancer cell types such as fibroblasts, immune cells like macrophages and lymphocytes, and epithelial cells along with their associated stroma [16]. The spread of cancerous cells from a primary cell to neighboring tissue is directly linked to cancer mortality. Because of this, finding methods to accurately evaluate and characterize cancer cells is utterly important for ultimately finding a treatment. Recently, within the past few decades, 3D modeling has become a preferred method for studying these processes, as these models present a more realistic form of modeling. The most common 3D platforms include the hanging drop method, spheroid formation, suspension culture such as bioreactors, magnetic levitation, bioprinting, and microfluidic systems, as are shown in Figure 2.5 [57-60]. Even though 3D modeling is capable of better mimicking different physiological states, it still comes with problems and limitations of its own.

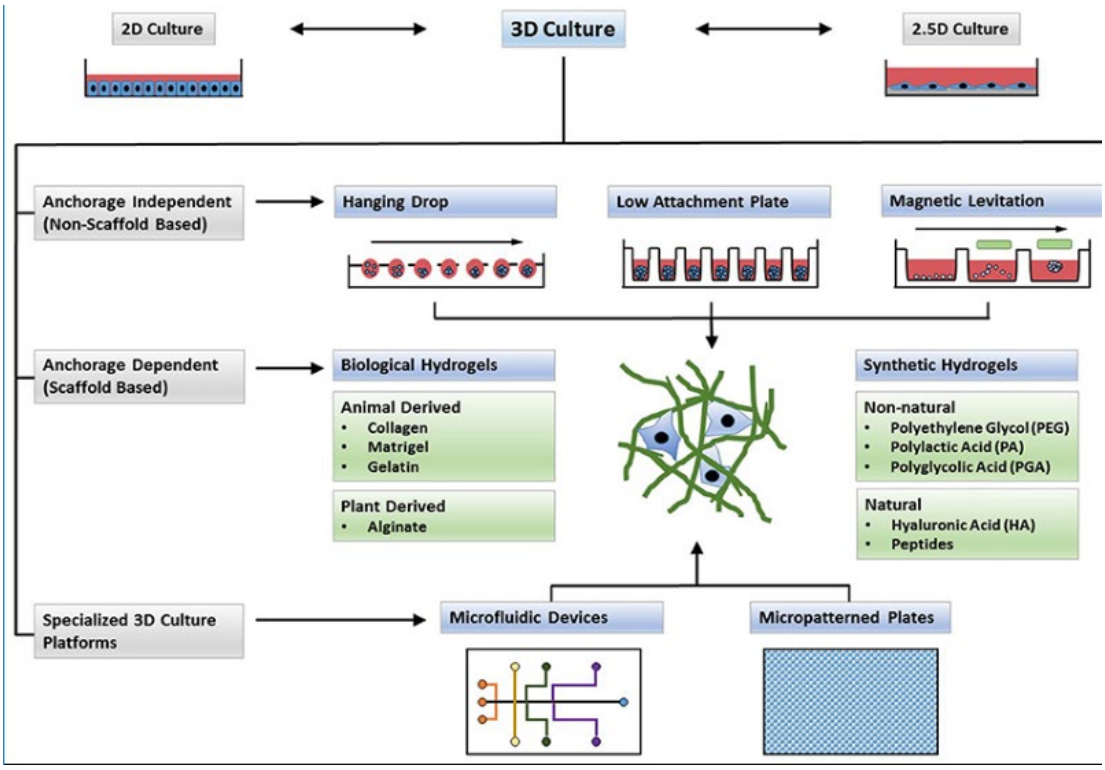

Figure 2.5. Types of 3D models in contract to 2D models [60]

As the cellular and structural complexity of a 3D system is increased, the accessibility of imaging and analyzing that data is decreased [61]. Currently, the most popular resources available for mimicking the 3D matrix of the breast consist of using hydrogel-based materials such as Matrigel® and collagen [41]. Due to their origin as animal-derived products, a major problem with these materials is batch-to-batch variability in biochemical and biophysical properties, as well as the lack in mechanical resilience [41]. A continuation of these issues can be seen when seeding cells for 3D culturing, where cells have the tendency of growing around or on the 3D hydrogel matrix surface and not being able to penetrate within a hydrogel structure due to poor architecture and highly acidic environments [62]. 3D bioprinting technologies using custom hydrogel-based bioinks allow a way for multiple cell types to be directly seeded into hydrogels with

the formation of any desired shape for tissue modeling. The ability of generating diseased or normal microenvironments, with tunable biophysical and biochemical properties and greater accuracy for complex structures, is crucial for developing tissue models with well-defined geometries [16]. Biological relevance and cell viability are the main desired factors when conducting experiments using tissue models to obtain the most realistic and physiologically relevant results.

2.5 3D MODELING OF BREAST CANCER

In vitro models are essential when evaluating breast cancer. *In vitro* cancer models are typically used to identify and evaluate cancer related processes, including tumor formation, tumor vascularization and angiogenesis, tumor cell metastasis and invasion, and drug screening [51, 63]. With this, scientists are able to create and assess cancer therapeutics before reaching the patient. With 3D modeling, researchers have the ability to reengineer and alter the tumor-like environment as we learn more about it. More specifically, there are various useful methods available for fabricating 3D models, including the use of scaffolds, hydrogels, microfluidic devices, and 3D bioprinting [64].

These 3D models are practical due to their diversity with the ability to create simple single celled constructs to complex multicellular models. This methods allows for the recreation of a tumors microenvironment without the use of a xenogeneic host or physiological irrelevant 2D models [65]. However, some of these models such as microfluidic devices and hydrogels only allow an unrealistic diffusion of oxygen and nutrients. This unregulated environment can alter the development of the overall tumor. Due to the small size and shape of tumor spheroids, the limitation of oxygen and nutrients

actually better reflects the tumor microenvironment in comparison to a fully oxygenated nourished layer [65, 66]. In addition, synthetic materials used for scaffolds create a barrier to the development of the native tumor microenvironment. As synthetic materials are not a natural matrix, it is not uncommon to see the cells acting differently on this foreign substance [65]. Various forms of 3D model systems have been used but each comes with limitations of their own.

3D bioprinting allows for the formation of structures that can support increased vascularization, while allowing for better scaffold designs with a multicellular platform [67-69]. 3D bioprinters come in three different forms: inkjet, extrusion-based, and laser-assisted, shown in Figure 2.6. A limitation related to the use of these bioprinters is their cost and size. Existing 3D bioprinters tend to be large and expensive with the one of lightest weighing about 14 pounds while costing upwards of $200,000 [19]. Typically, those with limited space and funds would not have access to this advancement.

Nonetheless, via 3D bioprinting techniques, the biological and biochemical components are able to be precisely positioned in a layered system. An innovation such as this has allowed others to use 3D bioprinting to fabricate numerous forms of mammalian tissue, tumors, and even organs [69-72]. Researchers working on breast cancer specifically found that through 3D bioprinting, complex tumors and bone matrices can be replicated [73]. These bioprinted models have proven to be representative of the breast cancer tumor with the development of good vascularization and a complex multicellular environment which can be used for *in vitro* drug screening [68, 74]. With this method, the biocompatibility, immunocompatibility, cell stability, and overall model

structure can be better ensured, making 3D bioprinting an attractive option for fabricating 3D tissue models.

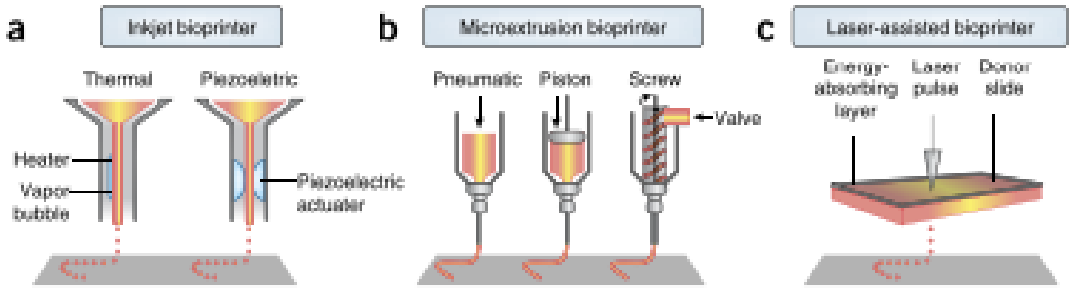

Figure 2.6. Different types of bioprinters

2.6 BIOINK: FABRICATION AND CHARACTERIZATION

A bioink is a substance used for printing the combination of cells and a biomaterial simultaneously [75, 76]. For 3D bioprinting, the selected bioink needs to be carefully characterized. The ideal bioink used in bioprinters will be one that is composed of naturally occurring or synthetic biocompatible biomaterials, such as commonly used hydrogel materials. Important aspects when selecting a hydrogel bioink include mechanical stresses, pH, chemicals required for use, viscosity, and how it crosslinks in order to assure cell viability [77, 78].

Predominantly, cancer models must be even more carefully constructed due to the complexity of the disease. Both the biophysical cues and the heterogeneous cellular components must be represented in the tumor microenvironment to have physiological compatibility [63, 68, 79]. For example, breast cancer cells have proven to react to the environmental stiffness they are placed in [80]. When looking for a bioink to replicate the breast cancer tumor microenvironment, a material that is able to mimic the stiffness of the

breast cancer tumor environment is crucial. In addition to the physical components, this designed microenvironment for printing must be multicellular and encourage the proliferation of cells. Structurally, the material needs to be porous to permit a diffusion of nutrients and oxygen while slowly degrading to enable an increase in surface area for the development of an extracellular matrix and cell proliferation.

Due to 3D bioprinting still being in its infancy, finding the ideal hydrogel composition for use as a bioink remains challenging. Thus, various materials or blends of materials have been investigated for this purpose. In this work, a blend of alginate and gelatin was determined to provide sufficient strength to maintain model structure, while allowing for cell proliferation and differentiation. The physical properties of gelatin, along with the ability to preserve cell viability using alginate was proposed for generating the optimal bioink that can be tuned to yield models with different stiffness properties to mimic the desired tissue of interest.

2.6.1 ALGINATE

Alginate is a naturally occurring polymer derived from seaweed [81]. Alginate hydrogels are currently being used for 3D cell models due to its wide availability and known chemical structure. Since large amounts of alginate can be fabricated through bacteria fermentation, alginate is typically low cost. In addition, the neutral pH of alginate supports cell viability. A hydrogel made from alginate can vary in elasticity, stability, and porosity based on concentration and type of alginates used [77, 82]. Crosslinking the alginate in calcium chloride for a sufficient amount of time will aid in the construction of a more complex cell-laden hydrogel structure. Because of the adaptability of alginate, it has

been used for other biomedical applications including wound healing, cell therapy, and bone grafting [77, 82]. A main issue that arises from the use of alginate hydrogels is the inhibition of proliferation and differentiation of some cells due to alginate lacking recognizable cell adhesion sites. This is why it is important to use RGD or other functional groups associated with cell adhesion with alginate to encourage cell proliferation. Retrieval of cells for data analysis from the alginate hydrogel is quick and easy through a simple de-gelling process [82]. The biocompatibility, high porosity construction, reversible control of stiffness, and favorable research conducted on regular 3D models has made alginate an ideal candidate for 3D bioprinting. As 3D bioprinting is currently becoming the adopted method to examine cell-to-cell interaction, growth, and differentiation finding a functional hydrogel bioink is critical for breast cancer modeling. Even though there are current bioinks that work meagerly, this proposed adaptable blend of alginate and gelatin will be low cost, have high biocompatibility, good biodegradability, elevated strength, adaptable rheological properties, and excellent cell viability.

2.6.2 GELATIN

Gelatin is a highly abundant natural gelling polymer derived from alkaline hydrolysis or by partial hydrolysis of collagen [83, 84]. Natural polymers in comparison to their synthetic counterpart are cheaper and have the tendency to better mimic components of the extracellular matrix (ECM) [85]. Gelatin is a favorable biomaterial because of its biodegradability, low antigenicity, and biocompatibility [86]. It is frequently used biopolymer in tissue engineering, pharmaceuticals, and even cosmetics. Porcine gelatin, specifically, is used for an abundance of biomedical applications due to its ability

to trigger hemostasis, ability to aid in tissue regeneration, and its antimicrobial properties [83]. Gelatin can also be used as a delivery system for controlled release of enhancers. Gelatin by itself has too low of a viscosity to be the only bioink component for printing and must be mixed with a more durable polymer as it will not self-sustain its structure for extended periods. Gelatin, unlike many other polymers, can be crosslinked through temperature regulation.

Finding a biocompatible and biodegradable hydrogel mixture appropriate for bioprinting is an obstacle many researchers are trying to solve. Blends of different natural and synthetic polymers have been proven to either maintain structure or be a viable microenvironment. Few composites have provided a structure and environment suitable for printing cell-laden tumor spheroids and even fewer have been used to mimic specific tissue types. An alginate-gelatin blend is one solution that has proven to be biodegradable, biocompatible, and non-cytotoxic to cell. Thus, this work will focus on use of an alginate-gelatin blend as bioink for fabrication of bioprinted tissues for studying breast cancer behavior.

CHAPTER 3

BIOPRINTING OF THREE-DIMENSIONAL (3D) TUMOR SPHEROIDS TO EVALUATE ADIPOCTYE-BREAST CANCER CELL INTERACTIONS

Chaji et al. Submitted to ACS Biomaterials Science & Engineering

ABSTRACT

Three-dimensional (3D) bioprinting, although still in its infancy as a fabrication tool, has the potential to effectively mimic many biological environments. Cell-laden 3D printed structures have demonstrated to be an improvement from the widely used monolayer platforms, largely because of recapitulation of native tissue architecture with the 3D structures. Thus, 3D *in vitro* models have been increasingly investigated for improved modeling of cell and disease systems, such as for breast cancer. While traditional 3D bioprinters can be large and expensive, this study aims to investigate the feasibility of modifying an affordable 3D printer for the bioprinting niche by applying a modified printer for studying breast cancer cell interactions. Specifically, while a correlation between obesity and breast cancer is known, the effects of adipocyte-secreted factors on breast cancer behavior are still not fully understood. In the present work, multicellular tumor spheroids comprised of adipocytes and breast cancer cells were bioprinted and evaluated. Cell viability and adipogenic maintenance post-printing were assessed to observe adipocyte-breast cancer cell interactions after 10 days. An ideal bioink of 3:2 5% alginate was determined to mimic the tissue stiffness observed in a physiological breast cancer tumor environment. Rheological characterization and degradation studies were performed to verify the stability of the artificial breast spheroid environment. It was found that both the breast cancer cells and adipocytes remained viable directly after printing and throughout the 10-day culture period within the tumor spheroids. Noticeably, the cell morphology and location changed when adipocyte and MCF-7 breast cancer cells were printed in co-culture, in comparison to being cultured by themselves. Overall, the goals of

this study were successfully accomplished as the feasibility of efficiently and economically fabricating multicellular bioprinted models of the breast tumor microenvironment using a modified low-cost 3D printer was established.

Keywords: 3D bioprinting, breast cancer, bioink, tumor spheroid, adipocytes, stem cells

INTRODUCTION

For many continuous years, breast cancer has paved the way as the second leading cause of cancer death in women in the Unites States [2, 87, 88]. Breast cancer is also the most commonly occurring cancer in women worldwide, and it is estimated that approximately 1 in every 8 women and 1 in every 1,000 men in the United States will develop invasive breast cancer [89]. These risks are even more detrimental for those who are overweight/obese postmenopausal women [44, 50]. In addition, the percentage of total fat volume in the breast can range from 7 to 56%, on average [90], indicating that adipose tissue makes up a large portion of the breast environment and as such, should be considered when studying breast tumor cell behavior. With the likelihood of obtaining breast cancer in one's lifetime progressively increasing, the importance for properly studying this disease has become vital. For decades, breast cancer has been evaluated using two-dimensional (2D) monolayer platforms despite 2D platforms lacking both the physiological and chemical cues represented in the *in vivo* microenvironment [51, 53, 91].

Mimicking breast cancer is challenging due to the various roles that different cells play. Structurally, the breast is comprised of adipose tissue, lobes, lobules, and ducts, which make up the fatty, fibrous, and granular tissues of the breast [90]. When combining these associated cell types (i.e., adipocytes, fibroblasts, mammary epithelial cells, etc.) in a 2D platform they have shown to behave differently than in a three-dimensional (3D) platform, with 3D platforms most resembling *in vivo* conditions and outcomes [64]. With appropriately designed 3D models, comparable physiological conditions can be achieved without the use of animal models; however, sufficient replication of native tissue is required for appropriate evaluation when studying a disease. For example, breast cancer

has been linked to body mass index due to the influence of adipocytes and their secretomes [92, 93]. These secretomes influence the upregulation of cancer production and cancer associated adipocytes [94, 95]. Co-culturing adipocytes with cancer cells has demonstrated an upregulation of osteopontin, TNF-α, IL-6, IL-1B, leptin, and adiponectin [96]. This upregulation of factors has resulted in increased breast cancer proliferation, including metastatic behavior. These hostile cells promote the production of cancer associated adipocytes, which then continue the deadly cycle [39, 97]. This is thought to be why postmenopausal women are 1.5 times more inclined to obtain breast cancer if overweight and 2 times more likely if obese [50]. Currently, however, there is no approach that allows scientists to accurately study these phenomena.

To overcome this limitation of suitable model platforms, 3D *in vitro* models such as formed using scaffolds, microfluidic devices, and 3D bioprinting have been developed to study breast cancer metastasis. At present, 3D bioprinting has emerged as a popular method for fabricating 3D tissue structures, as 3D bioprinters are advantageous due to their biomimicry capabilities [17]. Thus, we have determined this technique as ideal for printing the 3D breast cancer tumor environment, where resulting printed tissue structures would support cellular growth, cell-cell interactions and vascularization, while maintaining a supporting structure composed of comparable extracellular matrix proteins. Others have successfully demonstrated the interactions between cancer cells and neighboring cell types through the process of 3D bioprinting [68, 73, 79]. More specifically, MCF-7s have shown to be highly controlled and a promising cell type for tissue engineering, regenerative medicine, and drug screening applications when being bioprinted [98]. Overall, 3D bioprinters come in three different forms: inkjet, extrusion-based, and laser-

assisted [17]. The caveat of these bioprinters is the cost and size. Existing 3D bioprinters tend to be large and can cost anywhere from $10,000 to over $200,000 [19]. Typically, those with limited space and funds would not have access to this advancement. Therefore, this proof-of-concept study is intended to show the feasibility of 3D bioprinting the breast cancer microenvironment by converting a small low-cost 3D extrusion printer into a modified extrusion-based 3D bioprinter. This will be done by combining cells with a hydrogel that mimic the stiffness of breast cancer tissue in pursuance of producing a functional bioink.

3.2 MATERIALS AND METHODS

Materials

Alginic acid sodium salt and porcine gelatin (300g Bloom) were obtained from Sigma-Aldrich (St. Louis, MO, USA). Calcium chloride dehydrate was obtained from Fisher (Fair Lawn, NJ, USA). Deionized MilliQ water (18MΩ) was obtained from an in-house purification system. Adipose-derived stromal cells (ADSCs) and MCF-7 mammary adenocarcinoma cells (ER^+, PR^+) were obtained from the American Type Culture Collection (ATCC, Manassas, VA).

Bioprinter Optimization

A commercially-available extrusion-based 3D printer with attached syringe holder (Figure 3.1A) was used for this work (Tissue Scribe Gen. 3, 3D Cultures). Physical alterations were made directly to the printer along with adjustments to the CURA software settings to optimize this low-cost printer for printing cell-laden hydrogel tumor

spheroids. For optimal and efficient printing of the uniform tumor spheroids, a cylindrical design was created in AutoCAD (Autodesk, 2018), as shown in Figure 3.1B – C. The AutoCAD image was converted to an STL file and imported into the printer's CURA software for slicing.

CURA 15.04.2 consists of basic and advanced printing settings. The basic settings as follows: for quality, a layer height of 0.1mm and shell thickness of 0.7 mm were used, with the enable reaction box selected. For the fill settings, a bottom/top thickness of 2 mm and fill density of 10% were used. A printing speed of 130 mm/s was used along with a printing temperature of 37°C and a bed temperature of 0°C. The filament was assigned a diameter of 2.85 mm with 100% flow, as shown in Figure 3.1D.

Advanced settings consisted of nozzle size of 1.2 mm, retraction with a speed of 40.0 mm/s and distance of 4.5 mm. The quality settings were set to initial layer thickness of 0.3 mm, initial layer line width of 100%, cut off object bottom of 0 mm, and dual extrusion overlap of 0 mm. The multiple speed options were set at a travel speed of 150 mm/s, bottom layer speed of 20 mm/s, infill speed of 2 mm/s, top/bottom speed of 2 mm/s, outer shell speed of 2 mm/s, and inner shell speed of 2 mm/s. The cool for the printer had a minimal layer time of 20 s and enable cooling fan was selected.

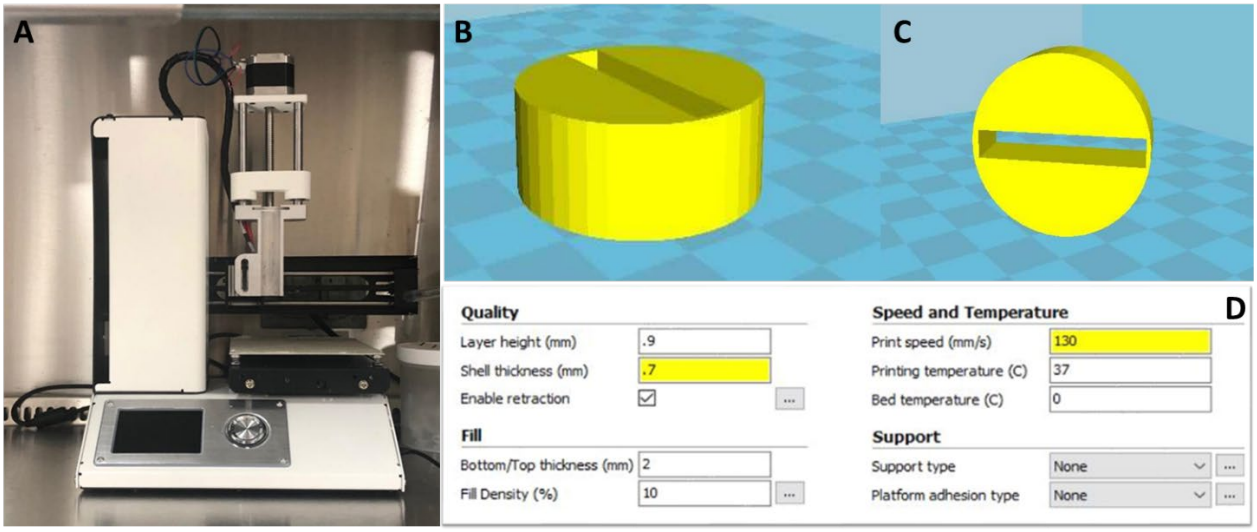

Figure 3.1. A) Extrusion-based 3D printer modified and used for bioprinting applications. B) AutoCAD design for 3D bioprinter. Cylinder sitting on x-axis design as printed. C) Cylinder rotated 90° off the x-axis. D) Basic settings calibrated for tumor spheroid bioprinting.

Hydrogel Bioink Screening

Initial screening to identify optimal materials for printing tumor spheroids was performed. Six different polymer materials, agarose, chitosan, pectin, alginate, gelatin and a blend of alginate and gelatin, were tested using solvents and crosslinkers as denoted in Table 1. Formed spheroids were prepared using the bioprinter and stored at 37℃. Resulting spheroids were incubated for up to 14 days and observations were made regarding maintenance of structure, degradation and cell viability post-crosslinking.

Spheroid Fabrication and Characterization

Based on the preliminary screening, a composite blend of alginate and gelatin was identified as the optimal hydrogel medium for tumor spheroid printing and used for all subsequent experiments. Composites consisting of various concentrations of alginate

(ranging from 3–5% w/v) and selected ratios of gelatin were tested to identify optimal crosslinking and extrusion properties for printing spheroids. Both the alginate and gelatin powders were first sterilized using ethylene oxide sterilization to decrease the chances of contamination while maintaining structural integrity of the tumor spheroids. All subsequent preparation and use of the hydrogel solution were carried out within a biosafety cabinet to protect the tumor spheroids from pathogens. To create both alginate and gelatin liquid solutions, the powders were dissolved in sterile deionized (DI) water for 2 hours at 40°C while stirring at a medium speed on a stir plate. The tumor spheroids initially tested were prepared using 3%, 4%, and 5% (w/v) alginate solutions that were mixed with a 50 mg/mL porcine gelatin solution, creating a 1:2, 2:1, 2:3, or 3:2 alginate to gelatin ratio mixture. Based on observations of crosslinking efficacy and degradation, the 1:2 and 2:1 composites were excluded from subsequent evaluation (data not shown). Prior to printing, the solutions were warmed to 37°C to support cell viability and ensure printability of the solution when extruded out of the syringe. The warmed hydrogel solution was printed into a 0.05 M calcium chloride crosslinking solution in a Petri dish. Once printed, the tumor spheroids were allowed to crosslink in the solution for 15 minutes. The calcium chloride was then removed and the tumor spheroids were rinsed with 1X Dulbecco's Phosphate Buffered Saline solution (PBS). Samples were then characterized to assess their resulting physical properties.

Rheological Characterization

Rheological properties of the printed spheroids were determined using an MCR 302 Anton Paar Rheometer (Anton Paar, Ashland, VA). A two-plate system was used

with a PP25/S plunger 25 mm in diameter in order to perform an amplitude sweep on each set of hydrogel spheroids. Six categories of hydrogel spheroids (2:3, or 3:2 alginate to gelatin ratios prepared using either 3, 4 or 5% alginate) were studied using rheology. For each category, four samples were measured, with each sample consisting of 40 – 45 hydrogel spheroids for measurement. The angular frequency was held constant at 10 radians/second, and the amplitude deflection angle was changed in intervals from 0.1% until 100% deflection. The temperature was held at a constant 37°C. Each sample was measured with a gap of 2 mm between the plates. The storage modulus, loss modulus and shear stress were all recorded for analysis.

Spheroid Degradation

Degradation of printed spheroids was observed to confirm an optimal ratio of alginate to gelatin. Preliminary evaluation with non-sterile prepared spheroids (using the previously described hydrogel combinations) helped determine the optimal ratio and concentration of alginate to gelatin, which was then evaluated using sterile prepared samples. For degradation studies, 10 tumor spheroid samples prepared using a 3:2 alginate to gelatin with 5% alginate, were printed and cross-linked in 0.05 M calcium chloride for 15 minutes. The samples were then rinsed and photographed on a stage at a height of 11.5 cm. Post-imaging, all tumor spheroids were placed in 2 mL of PBS (Ca^{2+} and Mg^{2+}-free) and incubated at 37°C and 5% CO_2 for 7 days. At the end of the 7-day period, the excess PBS was removed and tumor spheroid samples were photographed again at the same height. Image J software (2018, National Institutes of Health) was used to calculate the spheroid diameters and areas at both time points. Printed spheroid weight

before and after incubation was also recorded. This process was performed twice using different batches for both the non-sterile and sterile preparation to account for any batch-to-batch variability.

Scanning Electron Microscopy

Sample spheroids prepared using 3:2 alginate to gelatin with 5% alginate were fixed using 1 mL of formalin. Tumor spheroid samples were then placed in PBS and lyophilized for 24 hours. Dried samples were then gold-coated using a Leica EM ACE600 coater (Leica, Buffalo Grove, IL). After coating was complete, an FEI Teneo field emission scanning electron microscope (FEI, Inc., Hillsboro, OR) was used to capture images of the spheroids.

Cell Expansion and Seeding

MCF-7 cells, ranging from passage 7–15, were grown to confluence. ADSCs from passage 8–11 were grown to 95% confluence and then pre-differentiated into mature adipocytes for 7 days. Both MCF-7s and ADSCs were expanded using proliferation media consisting of low-glucose Dulbecco's Modified Eagle Medium (DMEM), 10% fetal bovine serum (FBS), and 1% penicillin/streptomycin (P/S), denoted as DMEM-Complete. Pre-differentiation of ADSCs into adipocytes was performed using adipocyte differentiation media consisting of high-glucose DMEM, 10% FBS, 1% P/S, 3-isobutyl-1-methylxanthine (IBMX), 100 µM indomethacin, 10 µM rosiglitazone, 0.02% dexamethasone, and 0.1% insulin.

Preliminary Screening of Culture Medium

A preliminary evaluation of cells cultured with DMEM-Complete (DC) or adipogenic maintenance media (AM) was performed to identify the optimal culture medium for supporting both cancer cell viability and maintaining the adipogenic characteristics of predifferentiated ADSCs. ADSCs and MCF-7 cells were seeded separately in 2D monoculture or in a co-culture with both cell types in the same well. Adipogenic maintenance media consisted of low-glucose DMEM, 10% FBS, 0.1% insulin, 0.02% dexamethasone, and 1% P/S. Cells were seeded at a seeding density of 7.6×10^4 cells/well for each condition, with a 50:50 ratio of MCF-7s to ADSCs used for co-culture conditions. Cells were cultured for 10 days and assessed at Day 2 and Day 10 of culture.

Bioprinting of 3D Cell-laden Tumor Spheroids

Cell-laden bioprinted spheroids containing either adipocytes or MCF-7 cells were first assessed to confirm optimal media formulation for 3D cultures. Cells were seeded at a total density of 5×10^5 cells/mL or 1×10^6 cells/mL for each condition, with a 50:50 ratio of MCF-7s to ADSCs used for co-culture conditions. A total of five tumor spheroids were printed directly into wells of 24-well Ultra-low Attachment plates (Corning, Tewksbury, MA), and samples were cultured for 10 days with fresh media replaced in the wells every 2–3 days. Following determination of optimal media formulation for 3D cultures, bioprinted spheroids containing a co-culture of adipocytes and MCF-7 cells were also printed using the same methods. Assays of cell viability, metabolic activity and lipid content were performed at Day 2 and Day 10 of culture to evaluate efficacy of printing and culture methods.

In Vitro Cell Viability and Metabolic Activity Assessment

Cell behavior was assessed for all 2D and 3D cultures after 2 and 10 days of seeding or printing. Cellular metabolic activity was assessed using alamarBlue® assay (Pierce Biotechnology, Rockford, IL). For this assay, 10% of the alamarBlue® working reagent was added to each well containing cells or tumor spheroids and incubated at 37°C for 8 hours and 24 hours, respectively. Media was collected and absorbance measured using a Biotek 800TS microplate reader (Winooski, VT) at 570 and 600nm. DNA concentration was determined using the Quant-iT PicoGreen® assay (Molecular Probes, Invitrogen, Eugene, OR) according to the manufacturer's protocol with slight modification. Cells or tumor spheroid samples were kept frozen at -80°C until used for the assay. Briefly, a series of freezing and thawing cycles, in combination with a Cyquant Cell Lysis Buffer (Invitrogen, USA), was used to lyse the cells for DNA quantification. Spheroids were dissociated using a 1:1 ratio of 0.2M sodium citrate solution and 1X cell lysis buffer. The spheroids were incubated in the dissociation solution for 10 minutes. Tumor spheroid solutions without cells were prepared using the same process and used for background subtraction. Cell viability was also qualitatively assessed for 3D cell-laden spheroids, using a LIVE/DEAD® Viability/Cytotoxicity assay (Molecular Probes, Invitrogen, Eugene, OR). Ethidium homodimer (EthD-) 1 and calcein AM were added to PBS to prepare a working reagent according to manufacturer specifications. Media was removed from each well and the tumor spheroids were rinsed with PBS. After rinsing, 0.5 mL of LIVE/DEAD® working reagent was added to each well containing tumor spheroids. The well plates were incubated at room temperature in the dark for 30 minutes before obtaining images. The images were collected using a Zeiss LSM 710 confocal

microscope (Zeiss, Oberkochen, Germany) using the Zeiss AXIO Observer Z1 microscope stand.

Adipogenic Potential

To quantify lipids present in the 2D cultures, Oil Red O (ORO) staining was performed. Cells were washed with PBS and fixed using 10% formalin. The wells were then washed with 60% isopropanol and allowed to dry. A stock solution of ORO was created by adding ORO powder (Sigma-Aldrich, St. Louis, MO, USA) to 100% isopropanol and stirring overnight. The stock solution was then filtered and diluted into a working solution by using 6 parts stock solution and 4 parts DI water. The working reagent was added to the cell cultures and incubated for 10 minutes at room temperature with gentle shaking on a rocker. Next, the wells were rinsed 4 times with DI water and images of the stained cells were captured. For quantification, absorbance of the ORO destained solution was determined. A volume of 500 µL of 100% isopropanol was added to each well and incubated for 15 minutes at room temperature to achieve destaining. The collected solution's absorbance values were measured using a Biotek 800TS microplate reader (Winooski, VT) at 500 nm. A solution of 100% isopropanol was used as a blank.

The adipogenic potential of the 3D tumor spheroids was assessed qualitatively using Nile Red staining. A 1 µM working solution of Nile Red was created by dissolving Nile Red powder (MP Biomedicals, Solon, OH) in small amounts of dimethyl sulfoxide (DMSO) and further diluted in 1X Hank's Balanced Salt Solution (HBSS). The tumor spheroids were incubated in the working solution for 15 minutes at 37ºC. The tumor

spheroids were washed with PBS and imaged with the Zeiss LSM 710 confocal microscope at 552 nm.

Statistical Analysis

All statistical analyses were performed using GraphPad Prism 6™ (GraphPad Software, Inc.) Two-way ANOVA followed by Tukey post-tests for multiple comparisons were performed to determine statistical significance between individual sample groups with significnace set at $p < 0.05$. Data are expressed as mean and standard deviation (SD).

3.3 RESULTS

Hydrogel Bioink Screening

The ideal bioink is one that can maintain its structure, has slow degradation over time, and can sustain viable cells after crosslinking. As shown in Table 1, only the alginate/gelatin mixture being crosslinked in 0.05 M calcium chloride was able to deliver the desired criteria, thus and alginate/gelatin composited was used for subsequent experiments.

Table 3.1. Polymers screened for spheroid formation.

Hydrogel Material	Solvent	Crosslinker	Structure Maintained (Y/N)	Significant Degradation Observed (Y/N)	Cells Viable After Crosslinked (Y/N)
Agarose	Deionized H_2O	None/Cooled PBS	Y	Y	Y
Chitosan	1% Glacial acetic acid	0.5 N Sodium Hydroxide	Y	N	N
Pectin	Deionized H_2O	1 M Calcium Chloride	N	Y	Y
Alginate	Deionized H_2O	1 M Calcium Chloride	Y	Y	Y
Gelatin	Deionized H_2O	None/Cooled PBS	Y	Y	Y
Alginate/Gelatin	Deionized H_2O	0.05 M Calcium Chloride	Y	N	Y

Rheological Characterization of Spheroids

Six different composites were used to prepare hydrogel spheroids, consisting of 2:3, or 3:2 alginate to gelatin ratios, prepared using either 3, 4 or 5% alginate. Analysis of the rheological properties for each of these composites showed that in the viscoelastic region, the storage modulus was higher than the loss modulus for all samples (Figure 3.2A and 3.2B). The yield point for all samples was around 1% strain, after which the internal integrity of the samples changed. Changes after 1% strain are not considered given that these samples did not undergo more than 1% strain during cell culture experiments. As shown by the obtained plots for both loss and storage modulus (Figure 3.2A and 3.2B), the loss and storage modulus were proportional to alginate concentration, where the loss and storage moduli increased as the alginate concentration increased. As shown in Figure 3.2C, the shear stress for each composite is also proportional to the

alginate concentration. The 3:2 5% alginate to gelatin alginate spheroids exhibited the highest storage and loss moduli, in addition to the highest resistance to shear stress. Shear stress any higher than approximately 205 Pa causes the structure of our hydrogels to change. Given that we use static culture, however, this did not pose a risk to our studies. The solution with the highest storage and loss modulus, 3:2 5% alginate to gelatin, was chosen for further studies and used for bioprinting experiments. The full rheological profile of the selected 3:2 5% alginate composite is shown in Figure 3.2D. The storage modulus for the 3:2 5% alginate to gelatin spheroids is much greater than its loss modulus.

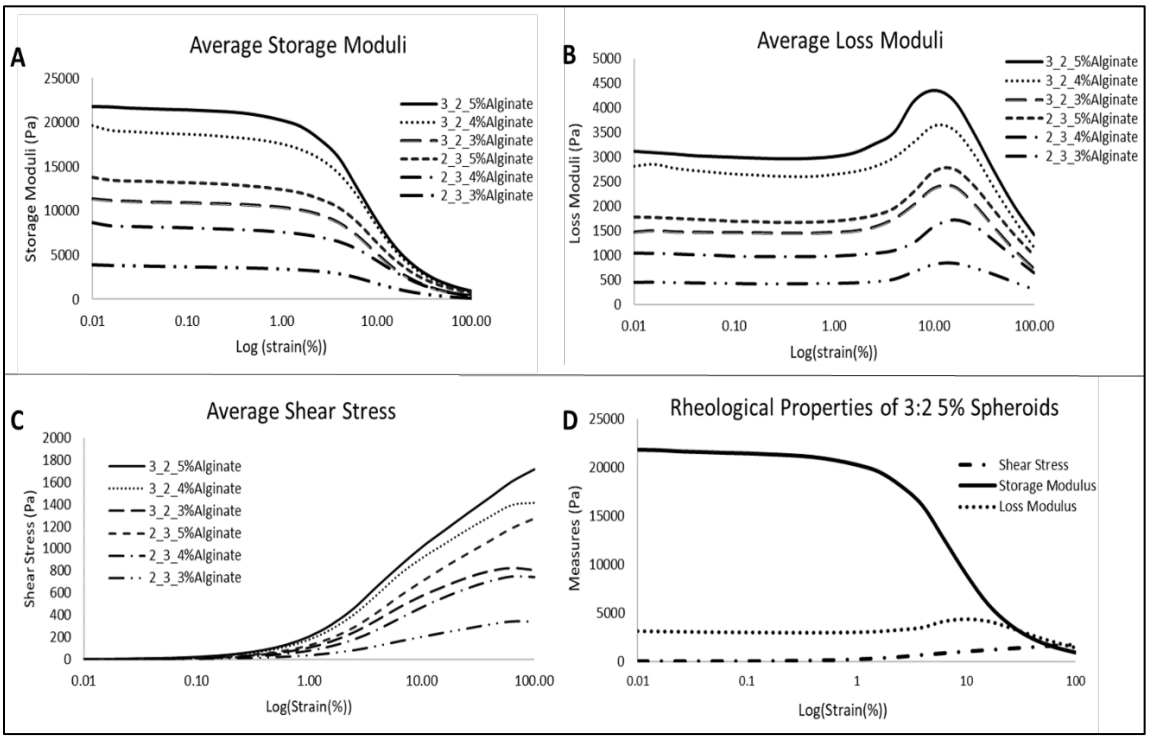

Figure 3.2. Average storage (A) and loss (B) moduli were measured for each tumor spheroid composite to determine the best material for printing cell-laden spheroids. Storage moduli and loss moduli were highest for the 3:2 5% alginate tumor spheroids. (C) Shear stress plot of the spheroids show 3:2 5% alginate spheroids with the most resistance to shear stress. (D) Rheological analysis of the chosen tumor spheroid composition. Storage modulus and loss modulus values show more elastic than viscous behavior. Shear stress values indicate that tumor spheroids cannot sustain large amounts of shear force.

Bioprinted Spheroid Degradation and Morphology

Tumor spheroids formed post printing are shown in Figure 3.3A. Tumor spheroid size was calculated using ImageJ software. The average diameter of the 3:2 5% alginate to gelatin tumor spheroids before degradation were 2117 ± 16.05 μm and 2214 ± 19.55 μm for Batch 1 and Batch 2, respectively. After incubation for the degradation study, the average tumor spheroid diameter was 2009 ± 14.50 μm and 2146 ± 11.32 μm, respectively. After 7 days of incubation for degradation analysis, the 3:2 5% alginate to gelatin spheroids retained approximately 96% of their diameter (Figure 3.3B). SEM was used to visualize the surface morphology of the printed spheroids. As shown in Figure 3.3C, the surface of spheroids maintained a rough texture due to crosslinking behavior. Minimal porosity was observed.

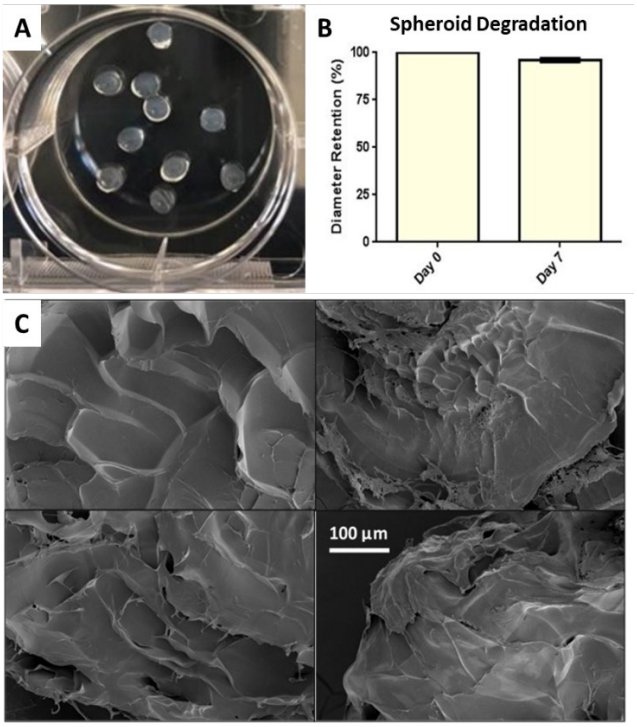

Figure 3.3. A) Representative image of bioprinted spheroids post-crosslinking. B) Diameter retention of 3:2 5% alginate tumor spheroids at Day 0 and Day 7. (D) Scanning electron microscopy images show the rough surface of tumor spheroids with minimal porosity.

Preliminary Screening of Culture Medium

2D Cell Viability and Metabolic Activity

Analysis of cells cultured in 2D monolayer were performed to determine optimal culture medium for co-culture conditions. Metabolic activity, determined by the alamarBlue® assay showed a statistically significant decrease in metabolic activity ($p<0.05$) for both media types from Day 2 to 10 for MCF-7s (Figure 3.4A) and no significant change in ADSC metabolic activity (Figure 3.4B). Measurement of DNA concentration using PicoGreen® assay showed a significant increase in DNA concentration for MCF-7s at Day 2 for the AM in comparison to DC (Figure 3.4D). For ADSCs grown in 2D, there was no significant difference in DNA concentration observed for any media formulation (Figure 3.4E). Co-culture of the ADSCs and MCF-7 cells together in 2D culture showed a significant decrease in metabolic activity from Day 2 to Day 10 for both the DC and AM media ($p<0.05$). However, there were no significant differences observed in DNA concentration for the co-culture samples using either media type (Figure 3.4F).

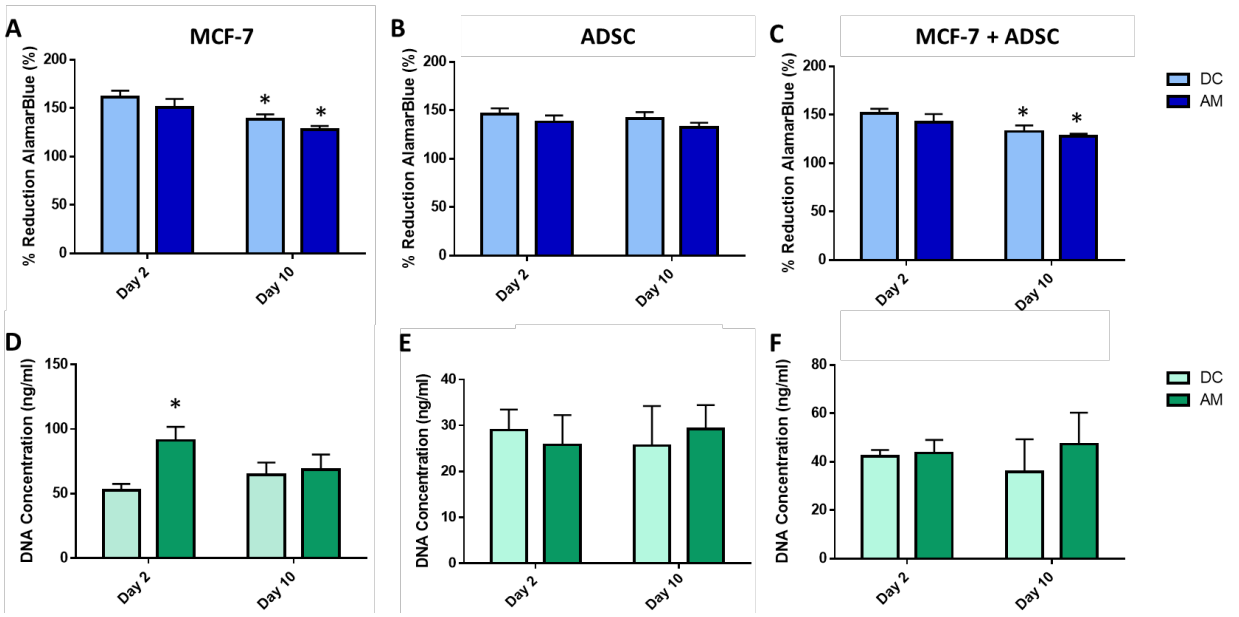

Figure 3.4. Cancer cell and adipocyte cell metabolic activity (as indicated by percent reduction alamarBlue® reagent) in monoculture (A and B) and co-culture (C) in 2D monolayer culture. DNA content as measured using PicoGreen® assay for MCF-7 cancer cells (D) and adipocytes (E) in monoculture and co-culture (F). Asterisks (*) indicate a statistically significant difference ($p<0.05$).

2D Adipogenic Potential

Representative cell morphology for MCF-7 and pre-differentiated ADSCs are shown in Figure 3.5A and 3.5D, respectively. The MCF-7 cells maintain their epithelial-like morphology, while ADSCs have visible lipid droplets present, indicating their differentiation to mature adipocytes prior to seeding and printing using the established differentiation media. ORO staining was used to confirm the presence of lipid droplets within the adipocytes. As shown in Figure 3.5B, no lipid is detected in the MCF-7 cells when stained with ORO, as expected. Lipid droplets are apparent, as shown in Figure 5E, for ADSCs differentiated to adipocytes. Quantification of the ORO destained solution showed little to no lipid for MCF-7 cells cultured with either media type (Figure 3.5C). There were greater amounts of lipid content measured for the ADSCs, however, no

significant difference was observed for ADSCs using either DC or AM media (Figure 3.5F). The 2D co-culture of ADSCs and MCF-7 cells showed that the ADSCs were still able to differentiate in the presence of the cancer cells, as indicated by lipids visible via ORO staining (Figure 3.5H) and confirmed by quantification of the destained solution. For the co-cultured cells, from significantly higher lipid content ($p<0.05$) was observed from Day 2 to Day 10 for the DC media (Figure 3.5I).

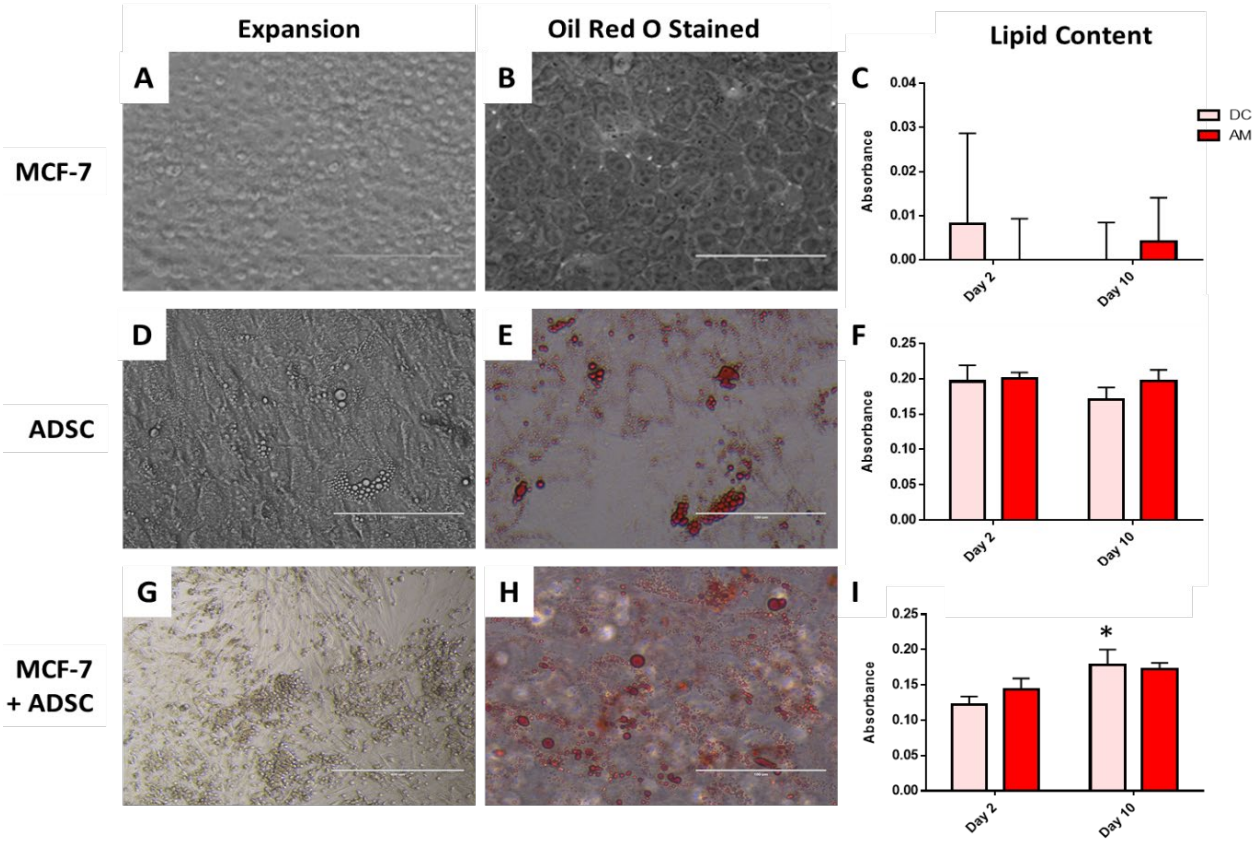

Figure 3.5. Expansion of A) MCF-7 cells, D) ADSCs and G) MCF-7 and ADSCs co-cultured after 10 days in 2D culture. B, E, and H show representative images of cells stained with Oil Red O to detect intracellular lipid produced following culture in adipogenic maintenance medium. The lipid content with respective absorbance values for each condition are shown in C, F, and I. Scale bar = 400 µm.

Evaluation of Bioprinted 3D Cell-laden Tumor Spheroids

3D Spheroid Monoculture Assessment

LIVE/DEAD® analysis showed that both the MCF-7s and predifferentiated ADSCs remained viable after 10 days post-printing within the tumor spheroids when cultured with both media types (Figure 3.6A-B and 3.6E-F). AlamarBlue® analysis to assess metabolic activity in the 3D platform showed no significant difference in metabolic activity for MCF-7s for either media type in 3D tumor spheroids (Figure 3.6C). The metabolic activity of the ADSCs was significantly less ($p<0.05$) at Day 10 than at Day 2 when cultured in the AM media (Figure 3.6G). PicoGreen® assay to quantify DNA content showed a significant increase ($p<0.05$) in DNA concentration for the MCF-7 cells cultured in DC media from Day 2 to Day 10 (Figure 3.6D). ADSCs, on the other hand, had a significant decrease ($p<0.05$) in DNA concentration from Day 2 to Day 10 when cultured in AM media (Figure 3.6H).

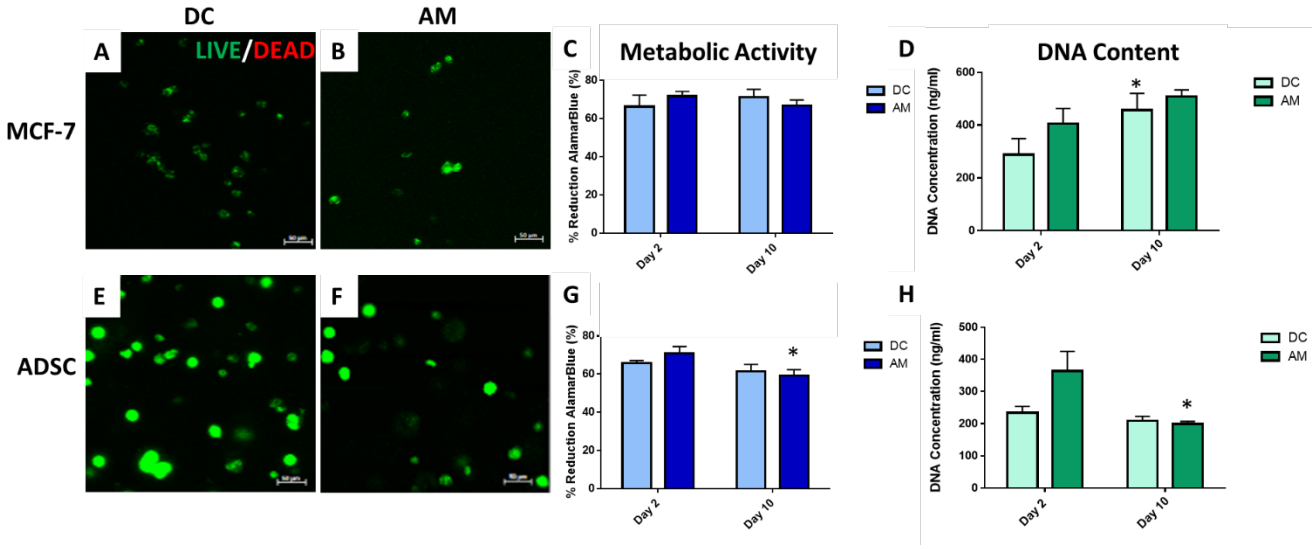

Figure 3.6. 3D monoculture assesment of MCF-7 and ADSC tumor spheroids in DMEM-Complete and adipogenic maintenance media. A-B & E-F) LIVE/DEAD® images. C-D & G-H) AlamarBlue® and PicoGreen® quantification of metabolic activity and cell viability. Scale bar = 50 µm.

Qualitative analysis of lipid presence for the 3D samples was conducted using Nile Red staining. Visualization of stained spheroids revealed no staining in MCF-7s with either media type (Figure 3.7A). Staining of the ADSCs showed the presence of lipids in ADSCs at both Day 2 and Day 10 when cultured in both media types.

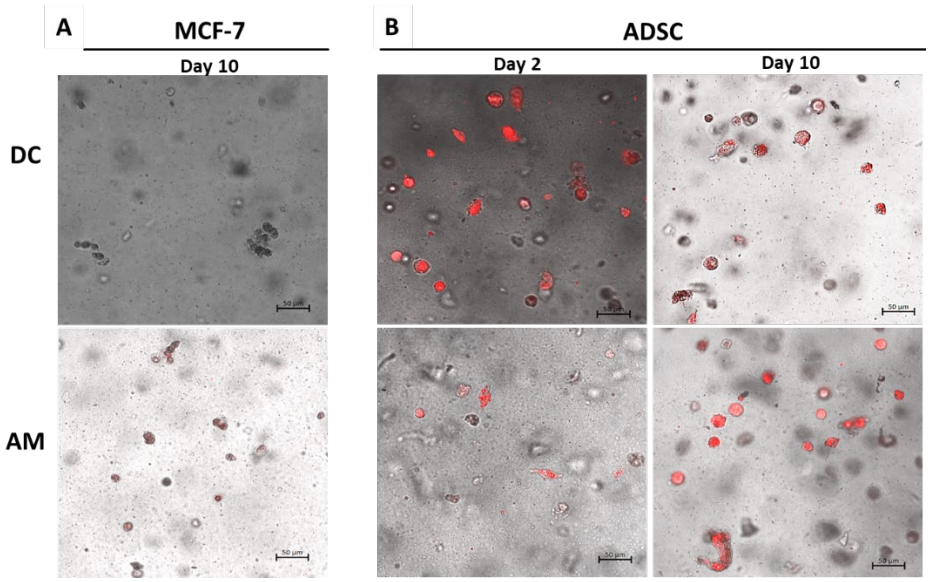

Figure 3.7. 3D monoculture Nile Red staining of lipids for A) MCF-7 and B) ADSC with DC and AM. Scale bar = 50 μm.

3D Spheroid Co-Culture Assessment

LIVE/DEAD® staining of tumor spheroids with co-cultured MCF-7 and ADSCs showed that the majority of cells remained viable after 10 days (Figure 3.8A-B). Non-viable cells, stained red, or necrotic cells (shown yellow in the overlay image) tended to be clustered together. As shown in Figure 3.8B, the confocal imaging topography map for the stained samples showed that the red-stained cells extended deeper into the center of the tumor spheroid. AlamarBlue® data indicated that a significant increase ($p<0.05$) in metabolic activity at Day 10 in comparison to Day 2 (Figure 3.8C), however, the DNA concentration determined by PicoGreen® assay showed no significant increase over time.

Evaluation of adipogenic potential, as indicated qualitatively with Nile Red staining, showed significant lipid presence in tumor spheroids with co-cultured MCF-7 and ADSCs at Day 10 (Figure 3.8E-F). The lipids in the 3D co-culture platform appeared more clustered together in comparison to the ADSCs alone shown in Figure 3.7B. Figure 3.8F shows the confocal imaging topography map of the lipids present in the co-culture environment, which reveals the depth of the lipids within the tumor spheroid environment.

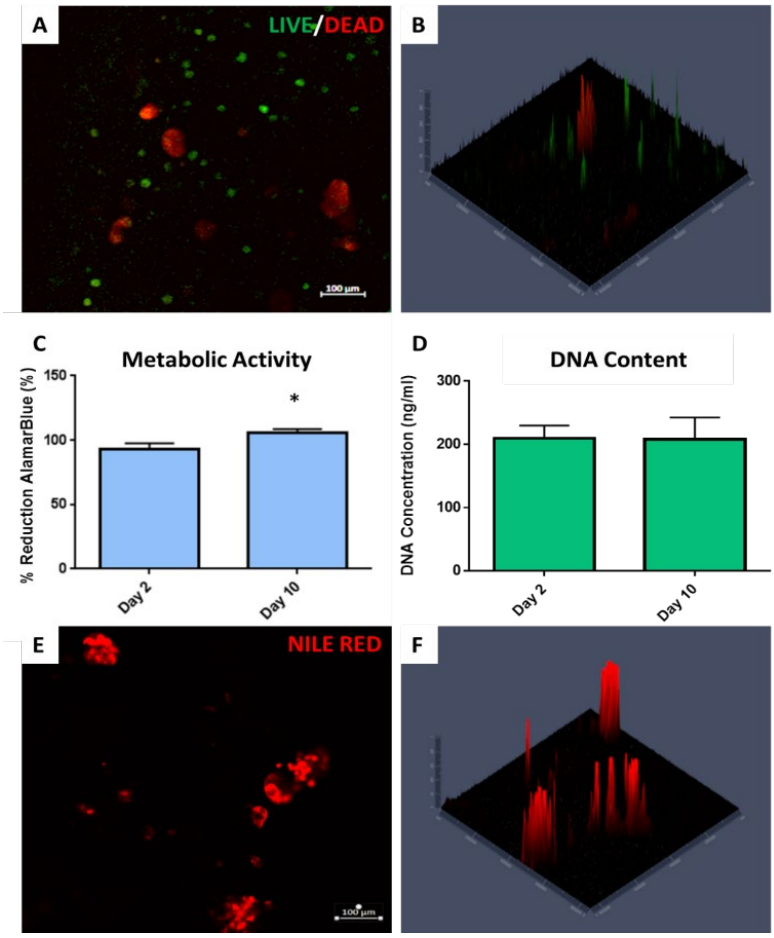

Figure 3.8. 3D co-cultured tumor spheroids. A-B) LIVE/DEAD® images with topography map. C-D) AlamarBlue® and PicoGreen® quantification of metabolic activity and cell viability. E-F) Nile Red staining of lipids with topography map.

3.4 DISCUSSION

Adipose tissue makes up the majority of the breast environment, which is comprised of ligaments, nerves, lymph vessels, lymph nodes, blood vessels, and connective tissue. This mammary adipose connective tissue consists primarily of adipocytes, making fat cells one of the top essential cell types in the breast cancer tumor microenvironment [20]. With mammary tissue being largely comprised of adipose tissue, which is characterized as a soft tissue, evaluating adipocyte-breast cancer cell interactions is essential to mimicking the mammary carcinoma environment [99]. Not only is maintaining the appropriate cell-cell interactions important, but the stiffness of any fabricated microenvironment will play a crucial role as well. While the elastic moduli for normal glandular and mammary adipose tissue have been measured to be between 2 and 66 kPa [100, 101], cancerous breast tissues have demonstrated increased stiffness up to seven times greater [102], with breast carcinoma having a mean shear stiffness 418% higher than the surrounding breast tissue [101]. These variations in stiffness of the breast cancer microenvironment have also been correlated to the specific cancer subtype, with triple negative and HER2+ tumors being stiffer [103]. Thus, to mimic breast tissue and cancerous breast tissue, the ideal tumor spheroid would have an elastic modulus value between 0.5 kPa and 25 kPa [100, 101].

For bioprinting, a key consideration is the bioink used for printing tissue structures. Hydrogels are optimal materials for bioinks because they can provide an easy way to facilitate a biocompatible 3D encapsulation structure. Hydrogels are also useful because they provide a permeable porosity that allows the exchange of media, nutrients, and waste associated with cell proliferation, which is essential to tissue engineering, organ-

on-a-chip, and drug screening applications [104]. Based on the physical properties of hydrogels, these materials are also well-suited for mimicking soft tissue, as is the goal of this work; thus, hydrogel biomaterials were selected for spheroid printing. Here, preliminary screening of various hydrogel materials showed the material construction, degradation, and rheological properties ultimately resulted in identification of an optimal composite of alginate and gelatin being selected for bioprinting.

It was essential for the bioprinted spheroidal structure to maintain its microenvironmental structure long enough for the culturing period with minimal degradation. Based on the results of both the degradation and rheological data, the concentration of 3:2 5% alginate to gelatin was selected for use to fabricated cell-laden tumor spheroids. With a higher storage modulus observed as compared to the loss modulus in the linear viscoelastic region, the analyses provides evidence that our materials are more elastic than viscous. Increased storage modulus can be associated with increased stiffness, which is most likely due to increased cross-linked chemical bonds.[105, 106] This is evidenced by the 3:2 5% alginate to gelatin spheroid as the increased alginate concentration allows for an increased number of cross-links between polymer molecules. Increased cross-links between alginate molecules yields a stiffer spheroid hydrogel that is more resistant to degradation, as evidenced in our degradation studies. Further, increased chemical cross-links provide more structural integrity, which affirmed the selection of the 3:2 5% alginate hydrogel for further studies.

As demonstrated by SEM images, the bioprinted tumor spheroids are not completely porous. The roughness of the spheroid surface suggests these spheroids could support good cell attachment, but this was not confirmed or essential in this work.

Future studies may include z-stack imaging of tumor spheroids to confirm this and also methods for introducing greater porosity into the tumor spheroids, while maintaining cell viability. This selected hydrogel composite was suitable as a bioink with optimal printability (i.e., extrusion from the syringe and needle) demonstrated. In addition, the alginate/gelatin composite provided adequate structural support for the tumor spheroid environment, while allowing for sufficient degradation in order to encourage cell proliferation. Rheological data specifically showed that this concentration, when crosslinked for 15 minutes in 0.05M calcium chloride, provided tumor spheroids with comparable soft tissue stiffness properties as reported for native breast cancer tissues.

For preparing cell-laden spheroids, in addition to selection of an optimal hydrogel bioink, it was equally important to determine optimal culturing parameters for the selected cells. Adipose-derived stromal cells were pre-differentiated to mature adipocytes for these experiments. Structurally, mature adipocytes have lipid-filled cell cytoplasms, with vast unilocular lipid droplets within the cell. In addition, these mature adipocytes are capable of secreting factors such as tumor necrosis factor- alpha (TNF-α), interleukin-6 (IL-6), and leptin [12, 107, 108]. Through early trials of the printing process, the fragile nature of these intracellular lipids was observed with the harsh stresses of bioprinting resulting in bursting or rupture of the adipocytes. In order to overcome this limitation and maintain the secretory potential of lipid-filled mature adipocytes, alterations to the printer and printing settings were conducted, as well as adjustments to the desired time and duration of pre-differentiation *in vitro*.

Differentiation media, as previously described above, was used to achieve adipogenesis, or conversion of ADSCs to mature adipocytes. However, the

dedifferentiation of adipocytes is a prevalent phenomenon that has been observed in response to physical cues, temperature fluctuations or other chemical cues.[109] Thus, to avoid this issue, a preliminary evaluation of culture media was performed. During the preliminary evaluation, all 2D cultures and tumor spheroids were cultured in differentiation media. The pre-differentiated ADSCs showed no signs of dedifferentiation, while the MCF-7s unexpectedly displayed abnormal signs of lipid presence, visible with Oil Red O and Nile Red staining (data not shown). This presence and formation of lipids within cancer cells has been previously shown as a response to high stress levels [110], thus indicating our need to optimize the culture conditions. Others have successfully studied the different forms of cancer behavior throughout the printing process and observed similar results [68, 111]. Subsequently, we then used a formulation of adipogenic maintenance media instead of differentiation media to maintain adipogenic phenotype for the ADSCs without yielding abnormal effects for the cancer cells in co-culture.

This maintenance media as described above, demonstrated the ability to prevent dedifferentiation of the differentiated ADSCs without provoking a stress response within the cancer cells. Overall, the use of DMEM-Complete and adipogenic maintenance media displayed no long-term significant difference for cell viability. However, when comparing cells cultured in 2D or in 3D cell-laden spheroids post-printing with either adipogenic maintenance media or DMEM-Complete growth media (previously used for expansion of both MCF-7 cells and ADSCs prior to differentiation), it was shown that the amount of lipid formed in differentiated ADSCs was maintained at a comparable level (when quantified with ORO) with just DMEM-Complete post-printing, thus the maintenance

media was not necessary and cells were sufficiently co-cultured in DMEM-Complete post-printing for subsequent analyses.

Cancer cells can react differently based on the stiffness of the environment in which they are placed [80]. Thus, identifying a tumor spheroid composition with the appropriate stiffness was essential for this study. The LIVE/DEAD® assay demonstrated that both the pre-differentiated adipocytes and the MCF-7s were able to remain viable with the selected printing alterations, indicating that the adjusted printing parameters were not too aggressive for cell viability. AlamarBlue® and PicoGreen® revealed the 3:2 5% alginate to gelatin hydrogel worked as a suitable bioink by maintaining cell viability for 10 days post-printing. The cells were able to proliferate and extract nutrients from the media through the hydrogel. Nile Red showed that lipids remained intact in the three-dimensional platform. Based on the Oil Red O staining it is expected that the lipid concentration in 3D increased over time as well, although this was not quantifiable with the Nile Red stain used.

Finally, with the 3D co-culture tumor spheroids containing both MCF-7 cells and pre-differentiated ADSCs, only DMEM-Complete was used as the media source for culture post-printing. The co-culture presented viable cells 10 days after printing, demonstrating survival of the cells under these printing conditions. The co-cultured cells had a tendency of moving closer to one another to form deep clusters within the innermost areas of the spheroids. The cells within these clusters seemed to fluoresce both green and red, suggesting some necrotic behavior. This occurrence is not atypical however, for breast tumors, where hypoxic conditions within the interstitial spaces of the tumor can affect cell viability [112], further demonstrating the physiological similarities of our

bioprinted tumor spheroids here and native breast cancer tissues. Even with LIVE/DEAD staining indicating some supposed necrotic behavior, there was an increase in DNA concentration and significant increase in total metabolic activity observed over time, indicating growth and activity of the cells during the culture period. The lipids within the 3D co-culture environment also tended to cluster closer to one another extending deeper into the tumor spheroid. The ADSC tumor spheroids displayed a more isolated dispersion of lipids while the co-culture showed them forming a bundle, suggesting an effect by the MCF-7 cancer cells on adipocyte behavior in the co-cultured samples.

3.5 CONCLUSION

With this proof-of-concept work, we successfully demonstrated the use of a low-cost modified printer for bioprinting of cell-laden tumor spheroids. We successfully recapitulated the 3D breast cancer tumor environment with intact adipocytes and breast cancer cells for evaluation. Thus, we have developed a platform with significant future clinical application. With modification, future application could entail bioprinting of a patient's specific breast cancer cells in conjunction with their own adipocytes for a high-throughput screening technique for identifying breast cancer treatment options. Future work will entail optimization of printed structures for modeling proliferation, migration, and metastasis influenced by adipocytes to improve methods towards developing a breast cancer cure.

ACKNOWLEDGEMENT

This work was supported by the University of Georgia Faculty Research Grant and It's the Journey, Inc. Breast Cancer Research Award. The authors thank Dr. Sergiy Minko and the Harbor Lights Endowment at the University of Georgia for equipment access.

CONFLICT OF INTEREST

Authors involved have no conflicts of interest. The authors are solely responsible for the writing and experiments conducted in the article.

CHAPTER 4

BIOPRINTING OF THREE-DIMENSIONAL (3D) HYDROGELS TO EVALUATE ADIPOCTYE EFFECTS ON BREAST CANCER CELL MIGRATION

Chaji et al. To be submitted to Journal of Biomedical Materials Research

ABSTRACT

With breast cancer remaining one of the leading causes of cancer death in women, there is increasing demand for the development of novel breast cancer cell/tissue models mimicking the breast microenvironment, which could be used for evaluating tumor cell behavior and screening of therapeutics. Specifically, triple-negative breast cancers, which lack the estrogen, progesterone, and HER2 receptors, are one of the deadliest forms of breast cancer due their metastatic abilities. In addition to the aggressive nature of triple-negative breast cancer, commonly modeled *in vitro* using MDA-MB-231 and HCC1806 cancer cell lines, triple-negative cancer can be further aggravated by neighboring tissues such as adipose tissue and the adipocytes that comprise this tissue. The secreted factors from these adipocytes, which make up their secretome, stimulate a feedback loop with the cancer cells encouraging the migration and proliferation of breast cancer. The increased presence of adipocytes in obese and overweight patients has been correlated to a more hostile feedback loop. The ideal model to evaluate the interactions between metastatic cancer lines and adipocytes would be three-dimensional model with the potential to appropriately mimic the chemical cues and physiological architecture found *in vivo*. This 3D model replication can be done through 3D bioprinting. By converting a low-cost extrusion-based printer into a 3D bioprinter, 3D printed tissue models can be recreated in an efficient and economical fashion. This project focuses on evaluating the migration of adipocytes and breast cancer cells in a 3D bioprinted breast cancer tumor environment. In this proposed study, we hypothesized that breast cancer cells will migrate towards the adipocytes in response to their secreted factors in the printed breast cancer

environment. Successful identification of migration, could yield knowledge about the link between breast cancer cell migration and metastasis with the presence of adipocytes. The three objectives of this work were to optimize the printer settings for a 3D layer-based migration platform, identify key secreted factors from cancer cells and adipocytes, and evaluate cell migration in response to these factors *in vitro*.

INTRODUCTION

Triple-negative breast cancer is a form of breast cancer that lacks expression of the estrogen receptor (ER-), progesterone receptor (PR-), and human epidermal growth factor 2 (HER2-) [5, 6]. This type of cancer is known to be one of the most aggressive types of breast cancer because of its difficulty to treat with receptor-targeting therapies and its ability to quickly proliferate and metastasize [5, 34]. Those with triple-negative breast cancer reportedly have higher rates of distant cancer recurrence and shorter survival periods [6, 34]. While triple-negative breast cancer is deadly enough, there are additional genetic and environmental factors that could worsen the aggressiveness of breast cancer [9]. A main contributor that may increase the risk of breast cancer in post-menopausal women is obesity, which creates an issue due to the large deposits of fat present in the body. Fat, also known as adipose tissue, is a soft connective tissue commonly located in the breast. This tissue is mainly comprised of fibroblasts, macrophages, and adipocytes. These adipocytes secrete factors such as adipokines, cytokines, and hormones that upregulate the production of cancer cells, creating a more aggressive breast cancer type [10]. Because of these effects, obesity has the tendency to lead to a faster tumor growth rate, less vascularization, increased hypoxia in the surrounding area, and the encouragement of epithelial-mesenchymal transition (EMT) [10]. Ultimately, obesity, thus, promotes the progression of triple-negative breast cancers, which are enriched by cancer stem cells. These aggressive breast cancer cells then promote an even deadlier cancer-associated adipocyte cell type, feeding continuation of the cycle. Often, the likelihood of death due to this type of cancer is as a result of the tumor cells' migratory ability. Triple-negative breast cancer commonly metastasizes to the

bone, brain, liver, and lungs. With upwards of 1.9 billion adults overweight or obese [113] in the world and breast cancer remaining the second leading cause of cancer death, the necessity of research that investigates this correlation is critical. Few have investigated the correlation between adipocytes and breast cancer in a 3D platform and even fewer have studied this link with various breast cancer cells obtained from different ethnicities.

4.2 MATERIALS AND METHODS

4.2.1 MATERIALS

Alginic acid sodium salt and porcine gelatin (300g Bloom) were obtained from Sigma-Aldrich (St. Louis, MO, USA). Calcium chloride dehydrate was obtained from Fisher Scientific (Fair Lawn, NJ, USA). Deionized MilliQ water (18MΩ) was obtained from an in-house purification system. Adipose-derived stromal cells (ADSCs), MDA-MB-231 cells (triple-negative breast cancer, $ER^-/PR^-/HER2^-$, Caucasian donor), and HCC1806 cells (triple-negative breast cancer, $ER^-/PR^-/HER2^-$, African-American donor) were obtained from the American Type Culture Collection (ATCC, Manassas, VA).

4.2.2 CELL EXPANSION AND EXPERIMENTAL PLAN

For expansion of each cell type (ADSCs, MDA-MB-231 and HCC1806 cells), proliferation media consisting of low-glucose Dulbecco's Modified Eagle Medium (DMEM, Gibco), 10% fetal bovine serum (FBS, Atlanta Biologicals), and 1% penicillin/streptomycin (P/S, Gibco), denoted as DMEM-Complete, was used. Cells were used for experimental analyses, as shown in Figure 4.1. ADSCs from passage 9 were grown to 95% confluence and then pre-differentiated into mature adipocytes for 15 days. Pre-differentiation of

ADSCs into adipocytes was performed using adipocyte differentiation media consisting of high-glucose DMEM, 10% FBS, 1% P/S, 3-isobutyl-1-methylxanthine (IBMX), 100 µM indomethacin, 10 µM rosiglitazone, 0.02% dexamethasone, and 0.1% insulin. MDA-MB-231 and HCC1806 cells, ranging from passage 13-14, were grown to confluence and used for seeding in co-culture experiments once ADSCs were differentiated.

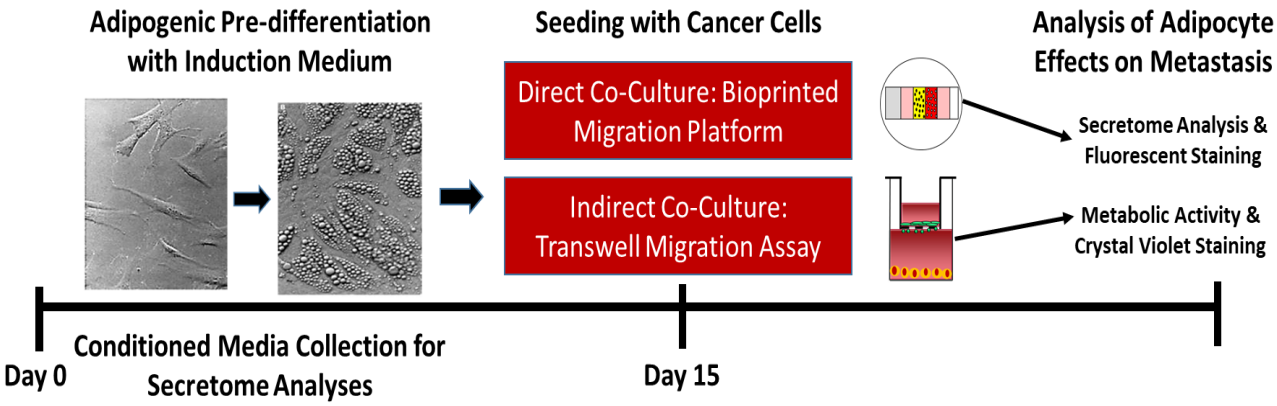

Figure 4.1. Schematic of experimental plan for direct and indirect co-cultures

4.2.3 CONDITIONED MEDIA SECRETOME ANALYSIS

Samples of conditioned culture media were collected throughout the ADSC differentiation process, and subsequently evaluated for production of three inflammatory markers: IL-6, leptin, and adiponectin. Specifically, samples were collected at Days 0, 3, 5, 7, 10, 11, 14, and 15 during the pre-differentiation period. Samples of media were also later collected from bioprinted cell-laden hydrogels seeded for direct co-culture of ADSCs and breast cancer cells (described below) and analyzed. Specifically, these samples consisted of media from cultures of MDA-MB-231 and HCC1806 cells alone or MDA-MB-231 and HCC1806 cells co-cultured with ADSCs. Samples of DMEM-Complete and

ADSC differentiation media were also evaluated as controls for comparison. Prior to analysis, all conditioned media samples were centrifuged for 20 minutes at 3,000 rpm and the supernatant was collected.

The detection of interluekin-6 (IL-6) was conducted using a QuickDetect IL-6 (Human) ELISA Kit (BioVision, Milpitas, CA, USA). Before preparing samples, 10 standards were prepared with the following concentrations: 48 pg/ml, 24 pg/ml, 12 pg/ml, 6 pg/ml, and 3 pg/ml. The first standard was created using a 1:1 ratio of the Standard Solution and the Standard Dilution, provided in the ELISA kit. Then, a series of serial dilutions were completed to obtain the other concentrations. With all solutions at room temperature, the samples were diluted by a dilution factor of 5 and gently mixed while being placed in the micro ELISA strip-plate. The samples and standards were covered with the plate closure film, and then incubated for 30 minutes at 37°C. Following incubation, the plate sealer was removed, and the solutions were washed 5 times allowing the for a 30-second rest period of the wash solution in between each wash. Next, HRP-Conjugate reagent was added to all wells except the blank and incubated for another 30 minutes at 37°C. Washing was repeated, as described above, followed by the addition of Chromogen Solution A and Chromogen Solution B, and incubation at 37°C in the dark for 15 minutes. Once completed, stop solution was added to each well to terminate the reaction changing the color of the solution from blue to yellow. Absorbance was read at 450 nm using a BioTek 800TS microplate reader (Winooski, VT) within 15 minutes of adding the stop solution. The blank control OD value was used for background subtraction.

A QuickDetect Leptin (Human) ELISA Kit (BioVision, Milpitas, CA, USA) was used to determine the concentration of leptin present in each sample. Before preparing samples, 10 standards were prepared with the following concentrations: 1350 pg/mL, 675 pg/mL, 337.5 pg/mL, 168.75 pg/mL, and 84.375 pg/mL. The first standard was created using a 1:1 ratio of the Standard Solution and the Standard Dilution provided in the ELISA kit. Then, a series of serial dilutions were completed to obtain the other concentrations. The samples were the same as listed above and were centrifuged for 20 minutes at 3,000 rpm. The samples were diluted by a dilution factor of 5 and gently mixed while being placed in the micro ELISA strip-plate. HRP-Conjugate reagent was added to the plate in the volume of twice the amount of the diluted sample. The solution was gently mixed and covered using a plate sealing film before incubating at 37°C for 60 minutes. Once completed, the plate sealer was removed, and the solution was aspirated and washed 5 times. A 1:1 ratio of Chromogen Solution A and Chromogen Solution B was added to the plate and mixed well before 15 minutes of incubation in the dark at 37°C. The stop solution was then added to terminate the reaction, changing the color from blue to yellow. The absorbance values were read at 450 nm using a Biotek 800TS microplate reader within 15 minutes of adding the stop solution. The blank control well was used for background subtraction.

A Human (Hu) Adiponectin ELISA Kit (Molecular Probes, Invitrogen, Eugene, OR) was used to determine the concentration of adiponectin present in the samples. To create the 18 standards, Hu adiponectin was reconstituted in 1 mL of deionized water, gently mixed, and allowed to sit for 15 minutes to ensure completion of reconstitution. This standard solution was labeled as 64 ng/mL of Hu adiponectin. To prepare the remaining

standards, 1 part 1X ELISA Buffer and 1 part from the highest concentration standard was added. This was done 7 times, and a blank consisting of 1 part 1X ELISA Buffer was added to the last tube. This gave adiponectin standard concentrations of 64 ng/mL, 32 ng/mL, 16 ng/mL, 8 ng/mL, 4 ng/mL, 2 ng/mL, 0.5 ng/mL and 0 ng/mL Hu adiponectin. The antigen was bound by adding 100 µL of the standard and the samples to the appropriate wells in the micro ELISA plate and incubating at 37ºC for 60 minutes with the plate being covered by a plate sealing film. The plate was then washed 3 times with 1X Wash Buffer. Once complete, 100 µL of the detection antibody solution was added to all wells except the chromogen blanks and incubated for 60 minutes at 37ºC with the plate covered. The washing step took place again, followed by the addition of 1X HRP solution and 60 minutes of incubation covered at 37ºC. The wells were then washed 5 times and the TMB substrate solution was added, turning the solution blue. The plate was incubated again in the dark for 20 minutes. Once finished, equal parts of stop solution was added to each well turning the blue pigment yellow. The Human Adiponectin ELISA absorbance values were read at a wavelength of 450 nm within 30 minutes of adding the stop solution.

4.2.4 BIOPRINTER SETUP

A commercially-available extrusion-based 3D printer with attached syringe holder was used for this work (Tissue Scribe Gen. 3, 3D Cultures). Physical alterations were made directly to the printer along with adjustments to its CURA software settings to optimize this low-cost printer for printing a cell-laden hydrogel layer platform. Instead of using AutoCAD software to create a printable design, printing was conducted directly from the printer itself, using its on-board controls. The x, y, and z directions were adjusted as

needed during the printing process, along with the extrusion function to output hydrogels in a rectangular shape to form the migration platform.

4.2.5 DIRECT CO-CULTURE: BIOPRINTING CELL-LADEN MIGRATION PLATFORM

As previously described, initial screening to identify optimal materials for printing was performed. A composite consisting of 3:2 5% alginate to gelatin was used as a hydrogel basis for fabricating the cell-laden migration platform for direct co-culture samples in this work. The cell-laden migration platforms were printed directly onto glass slides using a setup as shown in Figure 4.2 to evaluate interactions of MDA-MB-231 and HCC1806 cells co-cultured with ADSCs. MDA-MB-231 and HCC1806 cells cultured alone were used as controls for comparison. Prior to printing, slides were prepared by soaking in 100% ethanol for 5 minutes followed by flame sterilization. Once complete, the glass slides were autoclaved for 15 minutes. The 3:2 5% alginate to gelatin solution was prepared by sterilizing powders with ethylene oxide sterilization and dissolving in sterile DI water.

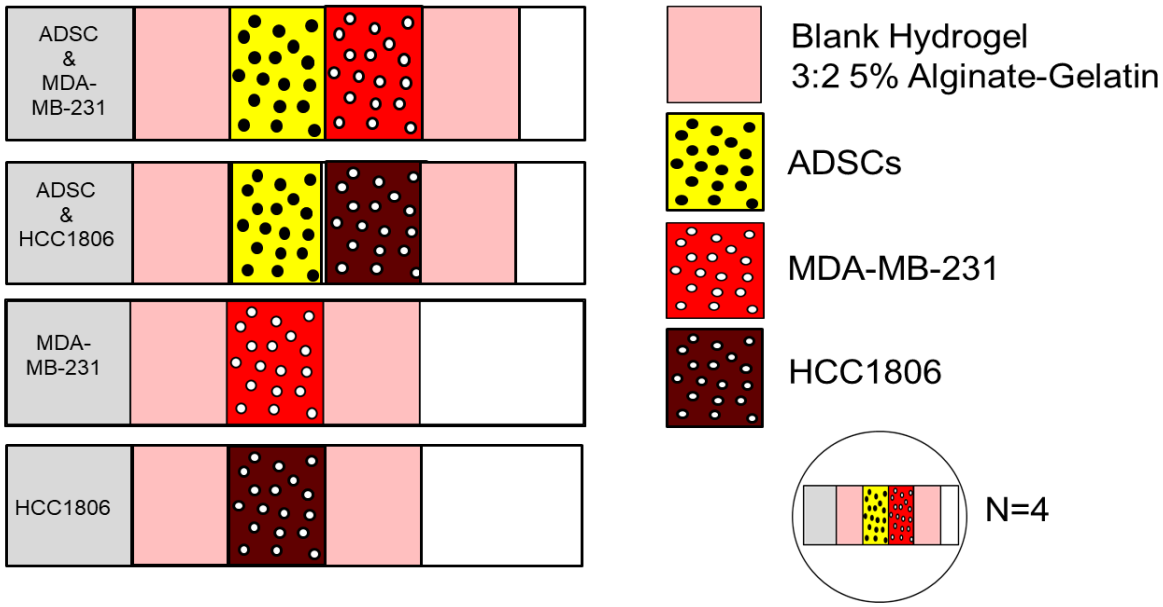

Figure 4.2. Setup for bioprinting of direct co-culture migration platform

Samples were printed once ADSCs were differentiated for the pre-determined culture period and cancer cells were confluent. Prior to printing, cancer cells were labeled using a CMFDA Green Cell Tracker with excitation and emission wavelengths of 492 nm and 517 nm, respectively (Molecular Probes, Invitrogen, Eugene, OR). Briefly, the powder was dissolved in dimethyl sulfoxide (DMSO) to obtain a concentration of 10mM. The stock solution was further diluted to a final working concentration of 3.5 μM in serum-free media. This working solution was placed into the desired flasks of HCC1806 or MDA-MB-231 cells and incubated for 45 minutes at 37°C. The working solution was then was removed and fresh media was added.

For printing, the cell-laden platforms consisted of a front layer of blank hydrogel, an ADSC layer (if co-culture sample), cancer layer, followed by another blank hydrogel layer (Figure 4.2). Hydrogels were crosslinked by drying for 30 minutes, followed by 15

minutes crosslinking in 0.05M calcium chloride. Cells were seeded at a total density of 1,000,000 cells/mL for the conditions without pre-differentiated adipocytes. Those with adipocytes contained 1,000,000 cells/mL of either MDA-MB-231 or HCC1806 cells and 1,000,000 cells/mL of ADSCs for co-culture conditions. A total of four platforms for each condition were printed directly onto glass slides, and the samples were cultured for 10 days with fresh media replaced in the wells every 2–3 days.

4.2.6 MICROSCOPIC ANALYSIS

Microscopic images of the bioprinted cell-laden hydrogels were captured at Day 2 using an inverted microscope with transmitted light (EVOS™ FLc Imaging System, ThermoFisher Scientific). Samples were later evaluated at Day 10 using fluorescent staining to visualize cells and cell-specific indicators, including DAPI staining for all samples and Nile Red for samples containing ADSCs to observe cell nuclei and to identify lipids present in the printed adipocytes, respectively.

DAPI Staining

The nuclei of all cells in the 3D cell-laden migratory hydrogels were stained using DAPI-Fluoromount-G (Electron Microscopy Sciences, Hatfield, PA, USA). This is a water-soluble blue nuclear fluorescent probe. The hydrogels were completely covered by the DAPI-Fluoromount-G and incubated at room temperature in the dark for 5 minutes before imaging using the EVOS FLc Imaging System.

Nile Red Staining

Nile Red staining was conducted to observe the presence of lipids (ADSCs) within the co-culture 3D migratory hydrogels. A 1 mM stock solution of Nile Red was created by dissolving Nile Red powder (MP Biomedicals, Solon, OH) in small amounts of DMSO; it was further diluted in 1X Hank's Balanced Salt Solution (HBSS) to a 1 μM working solution. The 3D migratory hydrogels were incubated in the working solution for 15 minutes at 37ºC and then washed with PBS before imaging with the EVOS FLc.

4.2.7 INDIRECT CO-CULTURE: TRANSWELL MIGRATION ASSAY

Cells were also evaluated using an indirect co-culturing approach making use of transwell inserts, as shown in Figure 4.3. Specifically, either MDA-MB-231 or HCC1806 cancer cells were seeded in the top of a transwell insert (Corning, Corning, NY), which was placed into a well of a multi-well plate. Cancer cells seeded in the top transwell insert were cultured with serum-free media. To compare the effects of ADSCs or ADSC-conditioned media, the bottom wells were seeded with either ADSCs pre-differentiated for 15 days or ADSC-conditioned media (collected at Day 15). Wells containing ADSCs were seeded with DMEM-Complete, while those seeded with ADSC-conditioned media received 50% conditioned media and 50% DMEM-Complete. Control samples were also seeded with only cancer cells in the top transwell insert and DMEM-Complete media in the bottom of the well. For evaluating cell viability, transwell inserts with 0.4 μm-pore size were used and placed with cells in 24-well plates. AlamarBlue® assay was then performed to measure metabolic activity, as an indicator of cell viability, for the samples in the 24-transwell plates. For evaluating cell migration, transwell inserts with 8 μm-pore size were

used and placed into 6-well plates. As an added sample for migration evaluation, in addition to the MDA-MB-231 samples that were previously described, another group was included for analysis to evaluate the effects of leptin on cell migration. The same conditions with the MDA-MB-231 cells and ADSCs or ADSC-conditioned media were used, but human leptin (>97%, recombinant, expressed in E. Coli, lyophilized powder, Sigma Aldrich) was also added to the bottom wells at a concentration of 30 ng/mL. Both alamarBlue® assay and imaging for migration evaluation were performed after 3 days.

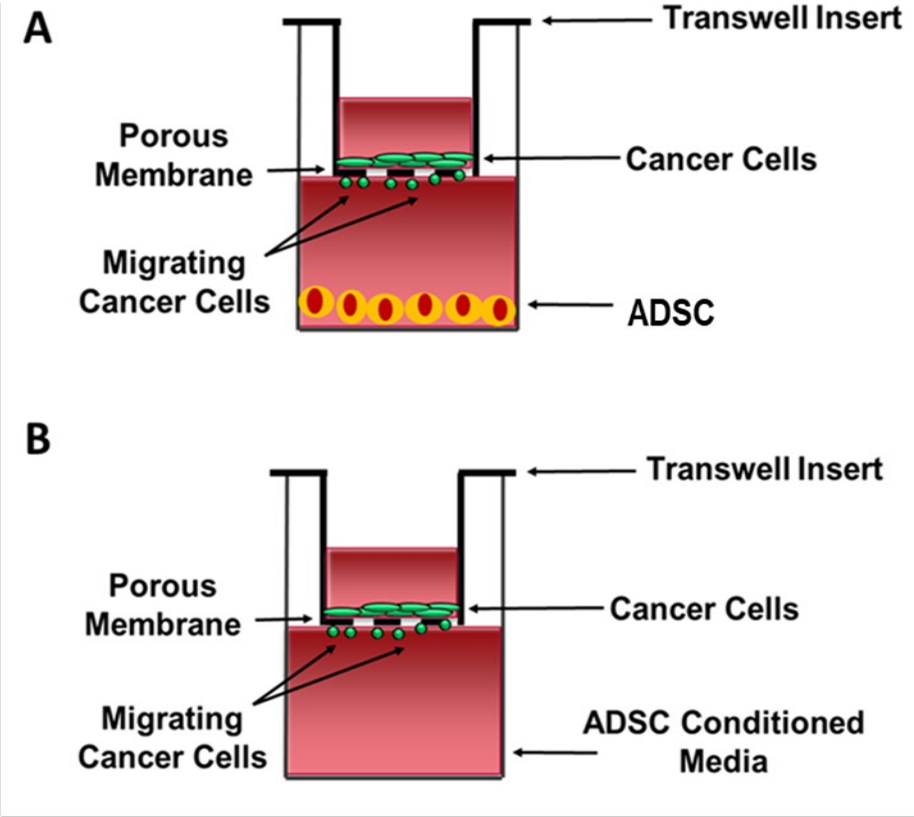

Figure 4.3. Schematic of transwell indirect co-culture setup used for analysis.

4.2.8 CRYSTAL VIOLET STAINING AND MIGRATION ANALYSIS

Crystal violet staining was conducted to evaluate cells that may have migrated through the porous transwell insert. The inserts were removed from the culture wells and placed into empty wells to gently rinse. Cells were then fixed using 1 mL of 10% formalin, followed by washing with 60% isopropanol, and allowed to dry. After the cells were fixed, a 0.5% solution of Gram's Crystal Violet (HIMEDIA, Mumbai, India) was created using 8 parts DI water and 2 parts 70% ethanol. The cells were then stained by soaking in the crystal violet solution for 3 minutes. The top of the transwell was then washed 3 times by gently dipping the insert into an empty well containing DI water. The inserts were then air dried and viewed under a microscope for imaging.

The bottom of each stained insert was viewed using an inverted microscope, and images were captured using the EVOS™ FLc Imaging System with transmitted light. A total of 3 images were captured for each insert at 4x, 10x, and 20x magnification. For analysis of migration, cells in each image were counted by three blinded reviewers using ImageJ (National Institutes of Health). The blind reviewers only counted the 20x magnification samples. The average number of migrated cells was then determined and reported for quantification.

4.2.9 STATISTICAL ANALYSIS

All statistical analyses were performed using GraphPad Prism 6™ (GraphPad Software, Inc.) One-way ANOVA followed by Tukey post-tests for multiple comparisons were performed to determine statistical significance between individual sample groups with significance set at $p<0.05$. Data are expressed as mean and standard deviation (SD).

4.3 RESULTS

Conditioned Media Secretome Analysis

The known concentrations of Human IL-6 Standard, Human Leptin Standard, and Human Adiponectin Standard as well as their absorbance values at a wavelength of 450 nm were used to prepare standard curves for each marker, which were used to determine concentrations of each protein in the collected conditioned media samples from pre-differentiated ADSCs.

Analysis of the condition media samples for the pro-inflammatory cytokine IL-6 (Figure 4.4A) showed a slightly lower amount of IL-6 detected in the differentiation control media in comparison to the DMEM-Complete media. Comparison of the Day 0 sample (at the onset of differentiation) showed a slight increase in IL-6 concentration when compared to the DMEM-Complete control. When comparing to the respective media type there was no significant difference ($p<0.05$) observed for any of the conditioned media conditions over the 15-day period. Next, the samples from each of the time points were compared to Day 0 to see the change in IL-6 over time. As shown in Figure 4.4B, the IL-6 concentrations from the background media is subtracted from the samples to observe the relative change in IL-6 over time, we see that there is an overall decrease in concentration from all time points in comparison to Day 0. Specifically, there is a statistically significant decrease at Days 5, 7. 10, 11, 15.

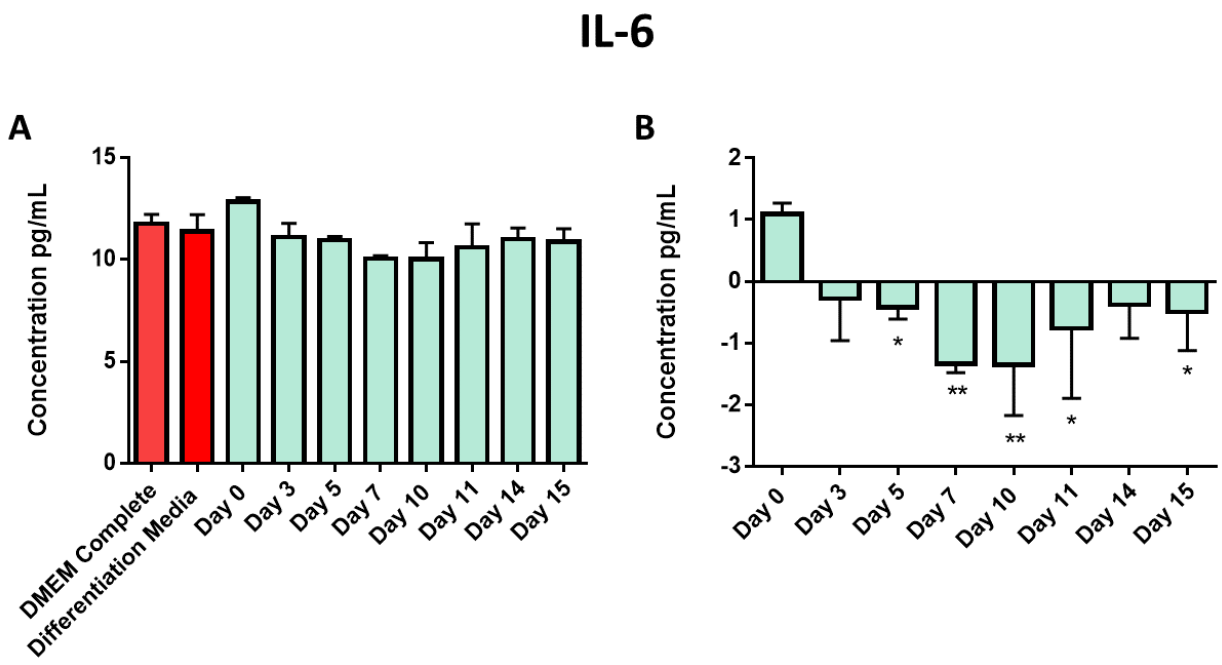

Figure 4.4. IL-6 protein concentrations measured in culture medium conditioned by ADSCs during pre-differentiation period. A) Measurements from samples over the 15-day differentiation period compared to control samples of DMEM-Complete and differentiation media without cells. B) Measurements from samples over the 15-day differentiation period after subtraction of background media compared to control sample at Day 0. Statistical significance ($p<0.05$) indicated with an asterisk (*) and multiple asterisks indicate greater statistical significance.

The conditioned media samples were assessed to screen for another pro-inflammatory cytokine, leptin. Figure 4.5A shows that there was a slight decrease in concentration of leptin in the conditioned media samples at different time points in comparison to the base differentiation media used. In addition, there was slight increase in leptin concentration from the base DMEM-Complete media when compared to the Day 0 sample, which was collected once ADSCs reached 95% confluence in proliferation media. As shown in Figure 4.5B, the base media leptin concentrations were subtracted from the respective sample time points to observe the relative change over time. This graph shows that there was a statistically significant decrease ($p<0.05$) for all of the

samples at each time points throughout differentiation in comparison to the amount of leptin present at Day 0. There is a greater statistically significant decrease in the samples at Day 10, 14, and 15 with the most statistically signifcant difference occuring at Day 7 of differentiation.

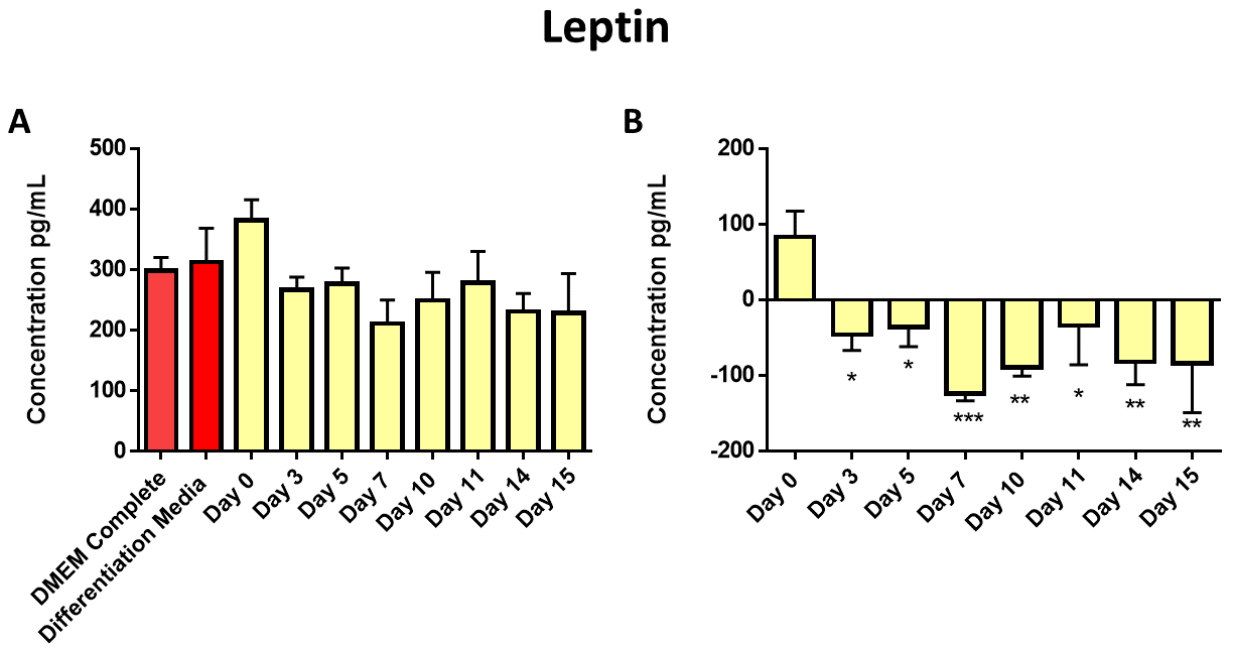

Figure 4.5. Leptin protein concentrations measured in culture medium conditioned by ADSCs during pre-differentiation period. A) Measurements from samples over the 15-day differentiation period compared to control samples of DMEM-Complete and differentiation media without cells. B) Measurements from samples over the 15-day differentiation period after subtraction of background media compared to control sample at Day 0. Statistical significance ($p<0.05$) indicated with an asterisk (*) and multiple asterisks indicate greater statistical significance.

In opposition to the pro-inflammatory cytokines, adiponectin is an anti-inflammatory cytokine that the conditioned media sampels were also screened for. Measurement of adiponectin protein (Figure 4.6) showed a statistically significant ($p<0.05$) increase of adiponectin in samples at Day 10, 11, 14, and 15 in comparison to the differentiation media control. As shown in Figure 4.6A, samples from Day 0, 3, and 5 showed little to no difference in comparison with their respective media type, with Day 7

showing a slight increase in adiponectin concentration. When comparing the differentiation conditioned media samples at different time points as shown in Figure 4.6B, there was a statistically significant increase observed at Days 10, 11, 14, and 15 in comparison with Day 0. The largest statistically significant increase in concentration for adiponectin was at Day 14, followed by Days 10 and 15.

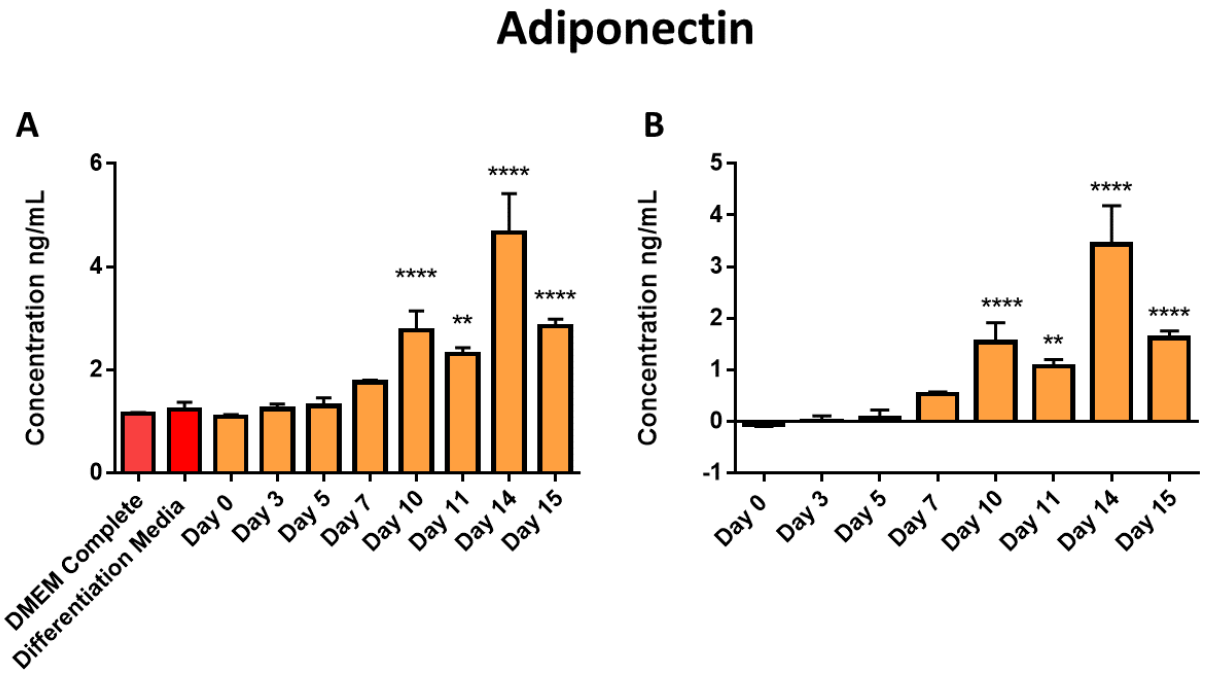

Figure 4.6. Adiponectin protein concentrations measured in culture medium conditioned by ADSCs during pre-differentiation period. A) Measurements from samples over the 15-day differentiation period compared to control samples of DMEM-Complete and differentiation media without cells. B) Measurements from samples over the 15-day differentiation period after subtraction of background media compared to control sample at Day 0. Statistical significance ($p<0.05$) indicated with an asterisk (*) and multiple asterisks indicate greater statistical significance.

Secretome Analysis of 3D Direct Co-Culture Samples

The concentrations of IL-6, leptin, and adiponectin were measured for conditioned media collected from cells cultured using the direct co-culture 3D migratory hydrogel

structures. Figure 4.7A shows that there was an increase in IL-6 concentration with the presence of ADSCs for both MDA-MB-231 and HCC1086 cells. While neither of these increases in IL-6 concentration was significant ($p<0.05$), the increase was larger for the MDA-MB-231 cancer cells. As shown in Figure 4.7B, evaluation of leptin expression showed a slight increase in leptin when comparing the MDA-MB-231 cells alone in the hydrogel with the MDA-MB-231 cancer cells co-cultured with pre-differentiated ADSCs. There is also a slight increase in leptin observed when comparing the control HCC1806 cells with the HCC1806 cells co-cultured with pre-differentiated ADSCs. While IL-6 and leptin both demonstrated negative concentration values, adiponectin showed positive concentrations for all conditions evaluated. As shown in Figure 4.7C, there was a slight decrease in adiponectin when comparing the MDA-MB-231 cells with the MDA-MB-231 cells co-cultured with the pre-differentiated ADSCs. The HCC1806 cells co-cultured with pre-differentiated ADSCs condition remained generally similar to the concentration of adiponectin in the HCC1806 control samples.

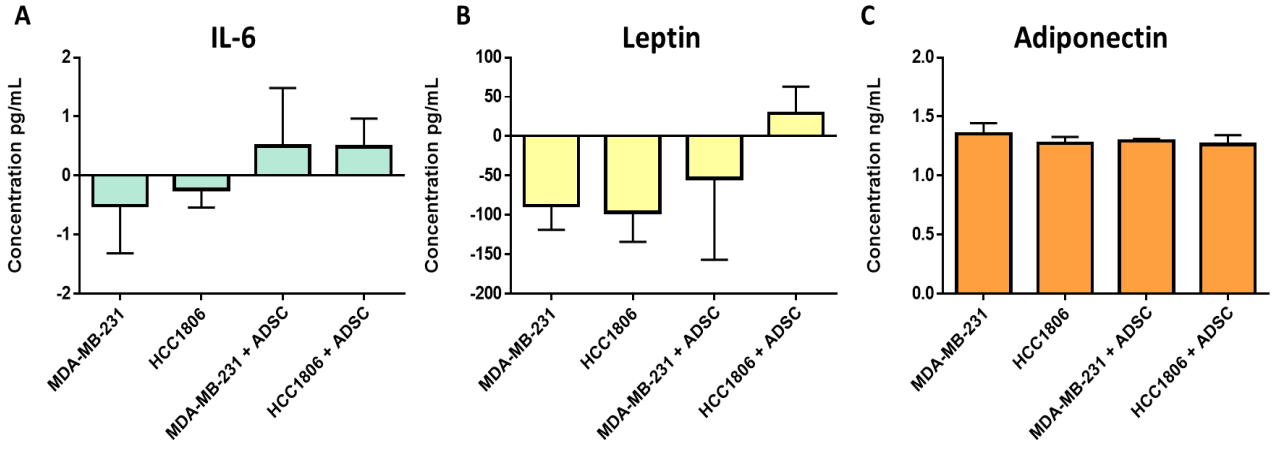

Figure 4.7. Evaluation of secreted cytokines from conditioned media collected from 3D direct co-culture samples in the hydrogel migration platform. Samples were evaluated to quantify expression of IL-6 (A), leptin (B), and adiponectin (C) by MDA-MB-231 and HCC1806 cells when co-cultured with ADSCs. Samples of each cancer cell type alone were evaluated for comparison.

Evaluation of Cancer Cell Migration in Bioprinted 3D Hydrogel Direct Co-Cultures

After placing the cell-laden hydrogels in culture, cells within the hydrogel platforms were imaged to assess cancer cell migration. Imaging was made difficult in some instances as the hydrogel either separated from the supporting glass slide or the hydrogel platform itself broke apart in other cases. At least partial imaging for all conditions was available at Day 2 with transmitted light. As shown in Figure 4.8, the cells remained in the printed partition. The MDA-MB-231 condition only remained as the cancer cell partition due to the separation of the hydrogel ends. The MDA-MB-231 cells co-cultured with ADSCs, sustained all partitions of the hydrogel blanks, the cancer cells, and the ADSCs. Both HCC-1806 and the HCC-1806 cells co-cultured with ADSCs, remained intact with all printed parts still connected. By Day 10, the hydrogels largely broke apart from one another making imaging even more difficult. Imaging for the HCC1806 cells co-cultured with the ADSCs was the only condition that could be fully imaged at Day 10 with all portions of the platform visible. The MDA-MB-231 cells co-cultured with ADSCs, HCC1806, and MDA-MB-231 cell-laden hydrogels were only able to retrieve partial imaging. As shown in Figure 4.9, the morphology of the HCC1806 cells co-cultured with ADSCs after 10 days demonstrated significant changes, as the cells migrated towards one another, with cells becoming larger and more round in shape.

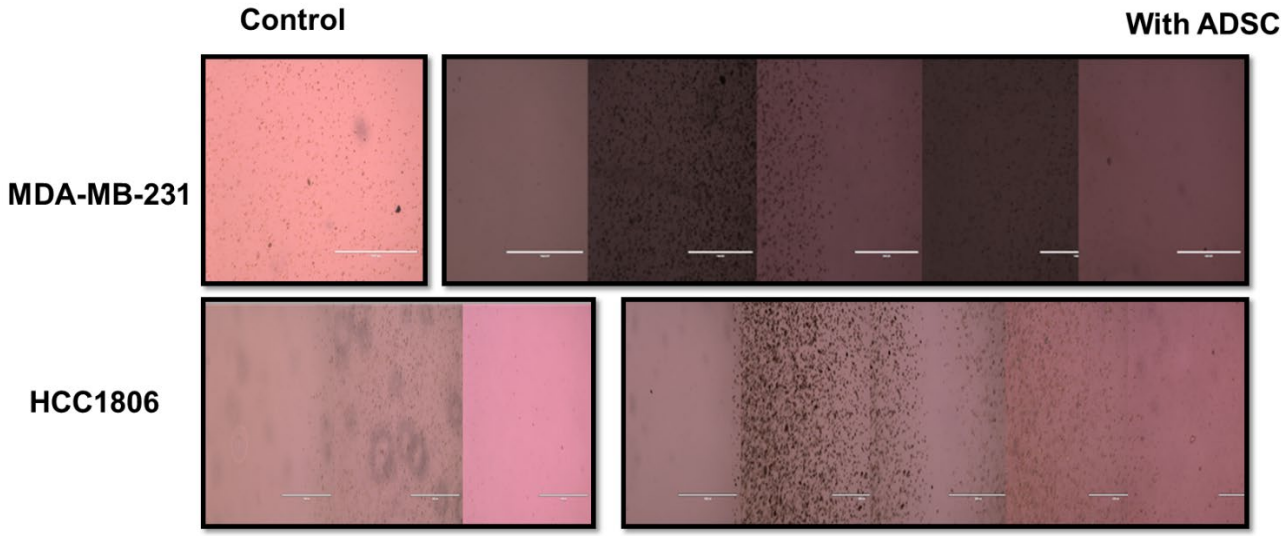

Figure 4.8. Direct culture 3D hydrogels at Day 2 of culturing left) control with the specific cancerous cell line and hydrogel blank. Right) co-culture with hydrogel blanks, cancerous cell line, and ADSCs.

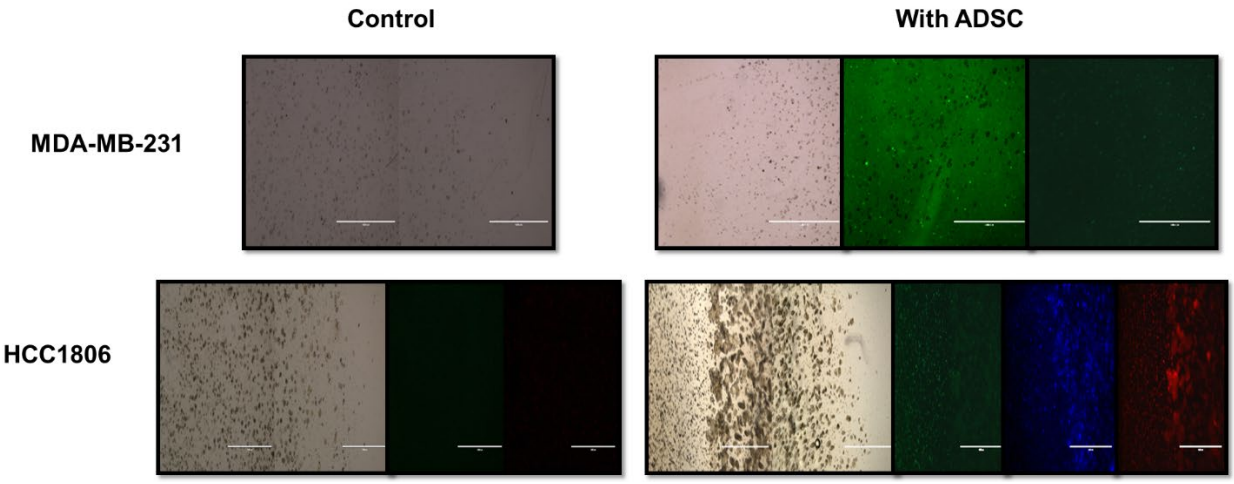

Figure 4.9. Direct co-culture 3D hydrogels at Day 10 of culturing. Green fluorescence is cancer cells labeled prior to printing; blue fluorescence is DAPI staining of cell nuclei; and red fluorescence is Nile Red staining of ADSC lipids. Left) control with the specific cancerous cell line and hydrogel blank. Right) co-culture with remaining hydrogel blanks, cancerous cell line, and ADSCs.

Evaluation of Indirect Co-Cultures with Transwell Inserts

Cells seeded in the transwell inserts were evaluated to assess metabolic activity and migration via an indirect co-culturing approach. Analysis of metabolic activity using the alamarBlue® assay was performed to compare the MDA-MB-231 and HCC1806 cancer cells cultured with ADSCs or ADSC conditioned media in transwell plates. As shown in Figure 4.10, there was no significant difference between any of the transwell conditions for either cell type. Little to no change in metabolic activity was observed when ADSCs are present on the bottom of the transwell plate with MBA-MB-231s. The MDA-MB-231 cells cultured with 50% conditioned media demonstrated a slight decrease in metabolic activity in comparison to the control. On the other hand, there was little to no difference in metabolic activity for the HCC1806 cells co-cultured with ADSCs and a slight decrease with the 50% conditioned media.

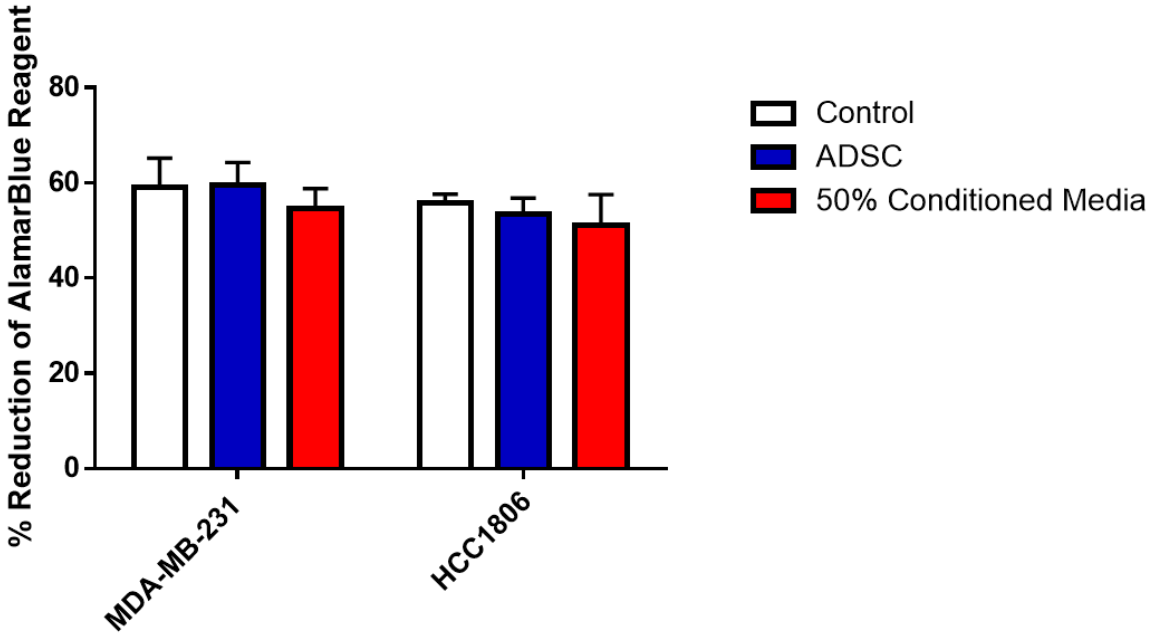

Figure 4.10. Metabolic activity of cells cultured using the indirect co-culturing transwell approach determined via alamarBlue® assay. No significant differences were observed between any conditions.

Evaluation of cells seeded for the migration assay showed cellular movement from one side of the transwell plate to the other for all condition types. Representative images of migrated cells stained with crystal violet are shown in Figure 4.11, with MDA-MB-231 cells shown on the top panel and HCC1806s images shown on the bottom panel. Cell migration was quantified by averaging cell counts performed by three blinded reviewers using the ImageJ software. An average of all values from the reviewers showed no significant difference in cancer cell migrations for any of the conditions evaluated. However, there is an obvious trend showing that the presence of conditioned media and ADSCs led to decreased migration of HCC1806 cells, while there was an increase in migration for the MDA-MB-231 cells. In addition, the MDA-MB-231 cells that were supplemented with exogenous leptin (added to wells with ADSCs or conditioned media) also showed an even greater increase in migration than those cultured without leptin added, although not significant. As can be seen in Figure 4.12B, the HCC1806 cells show opposing results, suggesting a downward trend with the presence of ADSC-secreted factors.

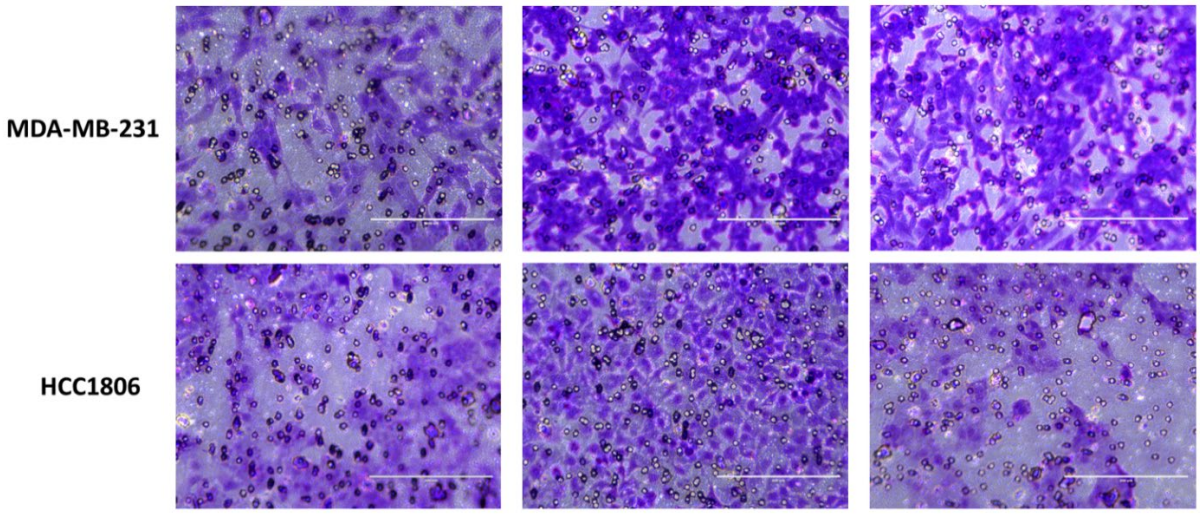

Figure 4.11. Representative images of transwell inserts evaluated for migration evaluation. Inserts were stained with crystal violet and images were quantified by counting with ImageJ, to evaluate MDA-MB-231 (top) and HCC1806 cells (bottom).

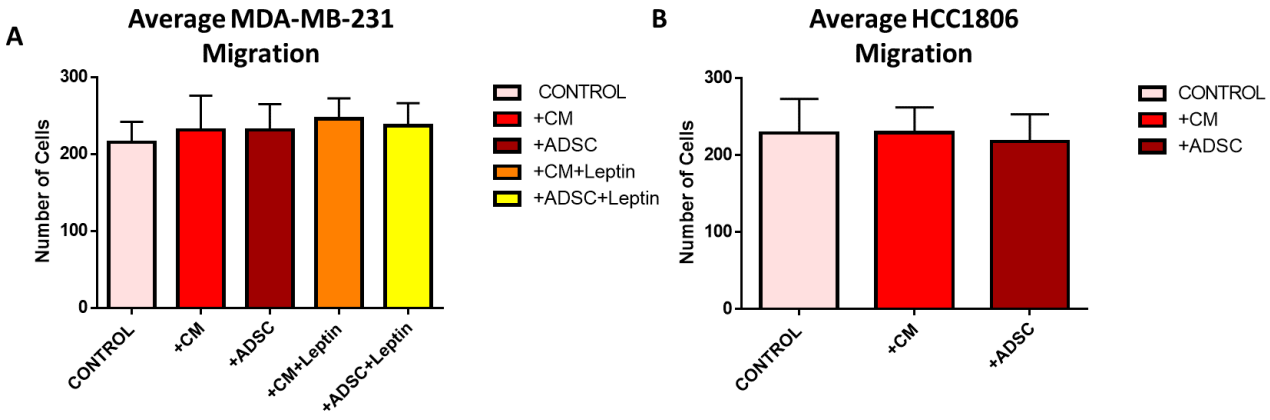

Figure 4.12. Quantification of cancer cell migration observed via indirect co-culturing with transwell inserts. No significant differences were observed, however interesting trends were noted for both MDA-MB-231 and HCC1806 cells.

4.4 DICUSSION

In addition to the cancer cells that may form, adipose tissue makes up the majority of the breast environment, which is comprised of ligaments, nerves, lymph vessels, lymph nodes, blood vessels, and connective tissue. This mammary adipose connective tissue consists primarily of adipocytes, making fat cells one of the top essential cell types in the breast cancer tumor microenvironment [20]. With mammary tissue being largely comprised of adipose tissue, which is characterized as a soft tissue, evaluating adipocyte-breast cancer cell interactions is essential to mimicking the mammary carcinoma environment [99]. In addition, adipocytes have been shown to work as an estrogen signal increasing the risk for breast cancer [41, 44]. Specifically, when working with triple-negative metastatic breast cancer cells, the migration is known to be correlated to

hormone levels *in vivo* [44]. As triple-negative breast cancer cannot be treated with general breast cancer therapies that target receptors, it is extremely important to be able to create a model that demonstrates the migration of cancer cells with the presence of adipocytes. By further understanding the cell migration and their secreted factors, advances will be made moving researchers one step closer to developing a specialized triple-negative breast cancer treatment.

Conditioned Media Secretome Analysis

Since the primary goal of this work was to evaluate the effects of adipocytes on breast cancer metastasis, it was important to characterize what biochemical factors the differentiated ADSCs were capable of producing. Specifically, we were interested in determining if three inflammatory markers that have been linked to breast cancer and associated with obesity were present in the differentiated ADSCs. Conditioned media collected throughout the 15-day differentiation process and 10 days after seeding our direct co-culture 3D hydrogels was, therefore, assessed for the presence of three inflammatory markers: IL-6, leptin and adiponectin.

Interluekin-6 (IL-6) is a cytokine that plays a major role in the behavior of breast cancer cells and adipocytes. IL-6 is an important cytokine due to its ability to aid the growth and differentiation of B cells [114]. These B cells are unique because they are the only eukaryotic cells capable of producing antibodies [114]. This pro-inflammatory cytokine is known to provide signals to initiate the inhibition of cell growth for various cell types, including breast cancer [114]. However, the addition of adipocytes has shown to significantly increase the migration and invasion of breast cancers which are ER-negative

as adipocytes secrete increased levels of IL-6 [115]. Studies have found that IL-6 is a cytokine, which can act as a pro-inflammatory or an anti-inflammatory depending on the surrounding conditions [116]. In addition, ADSCs have been shown to secrete much lower levels of IL-6 through the differentiation process and in monoculture in comparison to co-culture data sets [116]. Interestingly, ADSCs have shown the potential of differentiation to adipocytes, chondrocytes, osteocytes, myocytes, cardiomyocytes, and many other cell types [117-119]. One of the main differentiation factors to help initiate cardiomyogenic differentiation is IL-6 [117]. Because of this, it would be expected to see little production of IL-6 to ensure adipogenic differentiation. This is believed to be why there is a decrease in IL-6 concentration throughout the differentiation process when compared to the Day 0 baseline in our work here. The slight increase in IL-6 originating from the conditioned media and ADSC samples are thought to be a partial cause of the increase in migration observed throughout the transwell plate assay.

Leptin is a hormone, which is produced by adipose cells that regulate the energy balance in the body [119]. Leptin works by activating a receptor in the brain causing a decrease in food intake with an increase in energy expenditure [120]. In obese patients, there is a shown sensitivity decrease to leptin and the ideology of leptin resistance [120]. Leptin resistance is directly correlated to fat, with the goal of preventing reduction in body fat. This causes in increase in leptin with an increase in body fat [120]. In the case of the differentiating ADSCs here in our work, the differentiation media used contains high-glucose DMEM, working as the energy source. Without a need to increase energy from other locations within the cell, the leptin concentrations remain low and unneeded over time. This is also why the leptin concentrations are lower once the media source is

changed from proliferation to differentiation at Days 0 to 3 and onward. These findings are directly linked to the increase in leptin concentration when ADSCs were added to the two different cancer cell types in the co-culture samples. When the derived adipocytes are in contact with cancer cells, migration and secretions increase, causing an increase in the need for energy. Adipocytes store energy via triglycerides, which form into free fatty acids and glycerol after lipolysis. These free fatty acids and glycerol secrete fat-specific proteins such as leptin and adiponectin when energy is needed [119].

Similar to leptin, the expression of the hormone adiponectin is directly linked to adipose tissue, energy, and obesity [121]. Contrary to leptin however, adiponectin is an anti-inflammatory cytokine known for its role as an insulin stabilizer via glucose suppression [121]. Throughout the differentiation process, there are high levels of insulin available, more than what is typically needed by the cell. The ADSCs going through differentiation to adipocytes are likely trying to suppress these increased insulin levels. The more differentiated and adipocyte-like the cells become, the more they try to suppress the insulin by the increase of adiponectin production. This is why the levels of adiponectin are following an upward trend as the differentiation progresses. However, unlike leptin, levels of adiponectin are known to be reduced in obese patients [122-124], much like the slight decrease in adiponectin concentrations caused by the presence of ADSCs for our samples of co-cultured MDA-MB-231 or HCC1806 cells with ADSCs. Many others have found an inverse correlation between adiponectin levels and risk of breast cancer [125-129], ultimately linking obesity to breast cancer.

Evaluation of 3D Direct Co-Culture Bioprinted Hydrogels

For the direct co-culture samples consisting of ADSCs and cancer cells cultured together in a hydrogel platform, it was important to also evaluate cytokine expression as we aimed to determine the effects of these factors on cell migration. The data quantifying the cytokine concentrations in conditioned media from the hydrogel samples suggests that there is a slight increase in IL-6 and leptin concentration when ADSCs are present in the hydrogel. This data also suggests that the ADSCs are causing a slight decrease in adiponectin concentration for the MDA-MB-231 condition, with little to no change for the HCC1806 cells. While all the cytokines do not show a significant change in concentration between conditions, there could be significant amounts of IL-6, leptin, and adiponectin remaining in the hydrogel structure. The tested conditioned media samples came directly from the Petri dish post-incubation. Since the hydrogel itself was not physically disaggregated or lysed to release remaining secretory factors, large amounts could have remained embedded within the hydrogel. This phenomenon has been seen before with similar hydrogel structures made of collagen and ultimately could have the same effect in our study [130].

Images to evaluate cancer cell migration in the direct 3D co-culture hydrogels were obtained two days post-printing and after 10 total days in culture. Based on the images in Figure 4.8-4.9, not all sections of the hydrogel platform were able to be imaged. The 3D migratory hydrogel separated from the slide that the samples were originally printed upon and floated into the media within the Petri dish. Due to this movement, imaging the hydrogel was very difficult. In addition to separation from the glass slide, the 3D hydrogel also separated from parts of itself. The hydrogel was printed in 3 to 4 sections depending

on the condition seeded for a specific sample. Borders of the different sections (i.e. blank hydrogel section to cancer cell section) broke apart and migrated to different sections of the Petri dish. With the area available for observation of migration detached from the hydrogel, some of the cancer cells and/or ADSCs were likely forced to remain in their printed section, thus not able to migrate towards any chemotactic factors the ADSCs may have produced. However, by Day 2 there was still at least one intact hydrogel for the HCC1806, MDA-MB-231, and HCC1806 + ADSC conditions as seen in Figure 4.8-4.9. By Day 10 only sections of each condition remained. The MDA-MB-231 cells slightly migrated into open hydrogel space, while mostly remaining amongst one another. The condition with MDA-MB-231 + ADSCs separated, where we were not able to view the interaction between the cancer cells and the adipocytes. However, the cancer cell section of this condition had a similar migration pattern to that of the MDA-MB-231 cells alone by slightly moving into the open hydrogel space, but mostly remaining together. HCC1806 cells at Day 10 showed little to no migration into the blank hydrogel spacing. Lastly, by Day 10, small portions of the HCC1806 and ADSC interface were still connected in that direct co-culture sample. This conditioned showed a morphology change suggesting that the cancer cells and adipocytes migrated towards one another. Cancer cells were labeled prior to seeding with a green fluorescent molecule, DAPI staining was conducted on all cells, while Nile Red staining was used to identify lipids within adipocytes. Unfortunately, the staining for these caused all cells to fluoresce within the two different light filters, making it difficult to identify exactly which cell type was migrating.

Evaluation of Indirect Co-Cultures with Transwell Inserts

The results above showed there was little to no difference in metabolic activity for both MDA-MB-231 and HCC1806 cancer cells with the addition of ADSCs or 50% conditioned media. This can conclude that cells are not becoming any more or less metabolically active. Since the cell number and overall metabolic activity remained constant, this suggests that the cells are not migrating through the transwell plate due to lack of space. Thus, migration through the membrane of the transwell insert, is due to the chemotactic signals presented by either the ADSCs or conditioned media in the bottom section of the transwell plate. However, two different media types were used on the top and bottom of the transwell plates. The top consisted of serum-free media to limit the further proliferation of cancer cells, while the bottom contained either 50% conditioned media from differentiation media with the other 50% being DMEM-Complete or 100% DMEM-Complete with ADSCs. Regardless, the media type on the bottom of the transwell plate had additional serum proteins within it, and the FBS within the bottom media may have worked as an attractant to encourage cell migration from the top of the transwell insert membrane.

After evaluating the metabolic activity of these cells, migration was quantified. Cells were stained with a crystal violet staining solution and imaged. A set of 3 blinded reviewers counted the cells that migrated through the transwell plates, with results as shown in Figure 4.10. An average of the 3 counts was collected for each condition. For the MDA-MB-231 cells, there seemed to be a slight increase in migration of cells with the presence of 50% conditioned media, ADSCs, and leptin. The largest increases in migration occurred when leptin was added to the conditioned media and ADSCs, thus

suggesting that the addition of leptin stimulates the migration of cancer cells to other areas. In contrast to the MDA-MB-231 cells, the HCC1806 cells showed little to no migration with the presence of 50% ADSC conditioned media. The HCC1806 cells also demonstrated a decrease in migration with the addition of ADSCs. This suggests that the cytokines in the adipocytes interact differently with the HCC1806 cells and cause different fates. This is directly correlated to the importance of understanding how the ethnicity of the donors change the outcome of these interactions. From this, we can learn that different types and ethnicities of breast cancer show contrasting results.

4.5 CONCLUSION

In this study, we successfully used a low-cost modified printer for bioprinting of a cell-laden 3D hydrogel platform to study cell migration. We successfully identified concentrations of key secreted factors as ADSCs undergo differentiation to mature adipocytes, as well as quantities of secreted factors involved when cancer cells interact with adipocytes in a 3D platform. Migration of cancer cells was observed in direct co-culture via 3D bioprinted models as well as with indirect co-culture using transwell plate assessment. Cancer cell migration was attempted to be evaluated throughout the 3D bioprinting structure at different time points. The addition of ADSCs to the cancer cells increased migration for MDA-MB-231 cells, while decreasing migration of HCC1806 cells. Thus, the potential for creating a platform with patient-specific clinical applications has been realized. Much like the tumor spheroids reported in Chapter 3, with modification, this 3D migratory hydrogel structure could yield a larger platform to create a high throughput patient-specific breast cancer screening model for identifying treatment

options. Future work will encompass optimization of the slide-to-hydrogel adhesion, fluorescent staining of different cell types, and secretome collection methods to improve modeling with the hopes of developing a breast cancer cure.

CHAPTER 5

SUMMARY AND FUTURE WORK

Throughout the production of this work, we successfully modified a low-cost printer for the use of 3D bioprinting cell-laden structures: 3D spheroids and a layered hydrogel-based platform for studying cell migration. Both structures were able to support monoculture and co-culture conditions. The co-cultures included a combination of a cancer cell line of varying subtype, MCF-7, MDA-MB-231, or HCC1806, with ADSCs differentiated into adipocytes. The first step taken when working with these ADSCs was to decrease the differentiation time period. Originally, ADSC differentiation took approximately one month, and through the testing of various additives to the differentiation media, an updated protocol including rosiglitazone and indomethacin was created, shortening this period to about two weeks.

The poof-of-concept study described in Chapter 3 showed the feasibility of modifying the low-cost printer into a 3D bioprinter. We were able to create tumor spheroids with mechanical characteristics that mimicked that of breast cancer through the use of alginate and gelatin. In addition, cell viability and adipogenic maintenance in the 3D constructs were confirmed post printing, and after a 10-day culturing window, were compared to 2D platforms. Evaluation of the layered 3D hydrogel platform to study migration focused on the relationship between the adipocyte secretomes and cancer cell migration. Here, three key adipocyte-secreted factors involved in the cell-to-cell contact were assessed,

specifically evaluating pro- and anti-inflammatory cytokines. The pro-inflammatory cytokines (IL-6 and leptin) showed an overall decrease in concentration throughout the differentiation process, while the anti-inflammatory cytokine, adiponectin, showed an increase in presence. On the other hand, IL-6 and leptin demonstrated an increase in secretion when cancer cells interacted with the presence of lipids. These lipids were available in the form of pre-differentiated ADSCs. As was expected, adiponectin followed the opposite trend of the other cytokines by decreasing when cancer cells interacted with lipid proximity. The migration of the MDA-MB-231 cancer cells increased when conditioned media from differentiating adipocytes or pre-differentiated ADSCs were added to the bottom of transwell plates in the indirect co-culture platform. Surprisingly, the HCC1806 cancer cells showed a decrease in migration from the same stimuli. Imaging from the fluorescent staining concluded that the cancer cells and adipocytes migrated towards one another in the HCC1806 plus adipocyte condition after a 10-day culturing window. Migration in all other direct 3D migratory hydrogel cell conditions were inconclusive due to challenges that occurred throughout degradation processes. These proof-of-concept studies lay the foundation for personalized breast cancer screening and ultimately the creation of personalized breast cancer cures.

Recommendations for future work would be to establish additional modifications to the 3D bioprinter. Ideally the printer would have multiple syringe holder heads available for dual printing multiple cell lines simultaneously. Subsequently, the utilization of a larger syringe holder would increase the potential for creating larger structures. Currently, only a 5-mL syringe fits into the bioprinters syringe holder, so only small constructs can be made. In addition, an enclosure case with a stabilized temperature surrounding the 3D

bioprinter would significantly decrease the amount of time required for printing as well as aiding in the creation of layer-based structures.

In terms of printing more idealized tumor spheroids and migratory hydrogels, the printer settings need to be further adjusted to enhance the creation of smaller structures that will not overlap one another. Notably, the tumor spheroids were very difficult to image and there was no clear distinction of the different cell types. A recommendation for this study would be to label the cells and use z-stacks of confocal imaging. As desired above, while working with the transwell plates, there were two different media types used on the top and bottom portions. Subsequently, using serum-free media in both portions of the transwell will eliminate the possibility of the cells migrating due to the presence of proteins. Furthermore, the transwell plates were cultured for 3 days before cell viability and migration analysis. Hereafter, it would be beneficial to only culture these plates for 24-36 hours. Specifically, with the 3D layered hydrogel platform to study migration, there needs to be better methods for sterilization of the glass slides pre-printing. Even after 3 sterilization techniques the glass slides still had debris present on them. In addition, the glass slides need to be coated with an adhesion molecule that will prevent the hydrogel from detaching and floating off the slide. For staining purposes, we would like to find a stain that will only fluoresce in one specific color. The issue we came across was that the cells labeled using the green cell tracker also fluoresced in red when viewed under the microscope. This issue can be resolved by changing exposure time as well as the concentrations used. Lastly, the quantities of secreted factor from the 3D migratory hydrogels were low due to the entrapment within the hydrogel structure. In the future, the hydrogel should be dissolved using sodium citrate as discussed in the tumor spheroid

section of this work. This will allow for the complete degradation of the hydrogel structure and the release of all secreted products into the conditioned media.

Future studies are necessary to perfect this 3D breast cancer model. The assimilation of a few more cell types to create a more comprehensive model would be ideal. Incorporating the addition or subtraction of estrogen and progesterone levels within the printed structures would provide a greater understanding of how the breast cancer cells are interacting with other cell types and forming tumors. The integration of breast cancer therapeutics would further allow insight as to how certain cancer cell lines interact with specific medicines. This would ultimately create the desired personalized high-throughput screening technique.

CHAPTER 6

APPENDIX

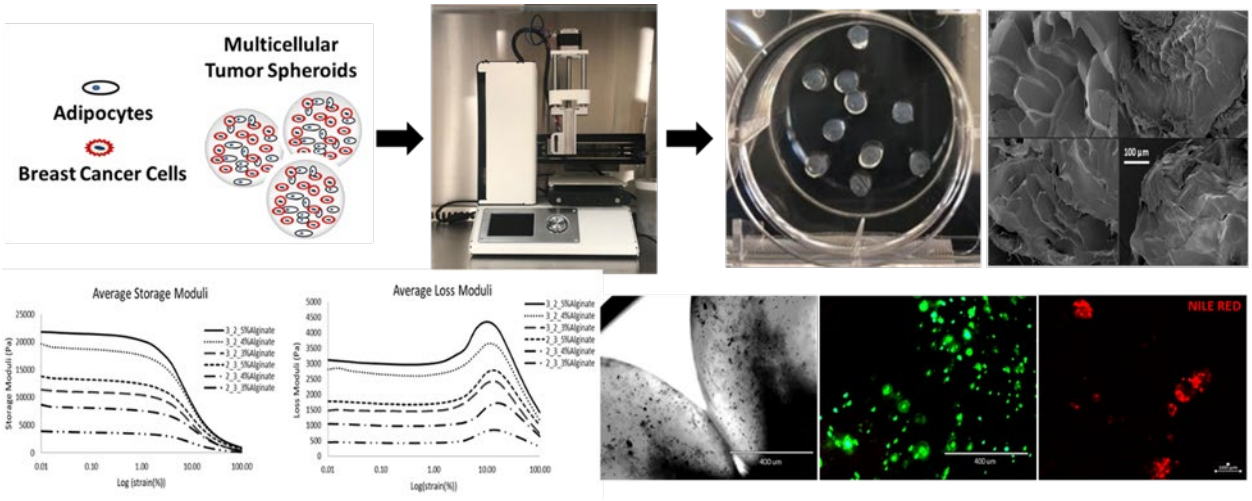

CHAPTER 7

REFERENCES

1. Bray, F., et al., *Global cancer statistics 2018: GLOBOCAN estimates of incidence and mortality worldwide for 36 cancers in 185 countries.* 2018. **68**(6): p. 394-424.
2. DeSantis, C., et al., *Breast cancer statistics, 2013.* 2014. **64**(1): p. 52-62.
3. DeSantis, C.E., et al., *Breast cancer statistics, 2017, racial disparity in mortality by state.* 2017. **67**(6): p. 439-448.
4. Oeffinger, K.C., et al., *Breast cancer screening for women at average risk: 2015 guideline update from the American Cancer Society.* 2015. **314**(15): p. 1599-1614.
5. Foulkes, W.D., I.E. Smith, and J.S.J.N.E.j.o.m. Reis-Filho, *Triple-negative breast cancer.* 2010. **363**(20): p. 1938-1948.
6. Liedtke, C., et al., *Response to neoadjuvant therapy and long-term survival in patients with triple-negative breast cancer.* 2008. **26**(8): p. 1275-1281.
7. Selzner, M., et al., *Liver metastases from breast cancer: long-term survival after curative resection.* 2000. **127**(4): p. 383-389.
8. Hortobagyi, G.N., et al., *Management of stage III primary breast cancer with primary chemotherapy, surgery, and radiation therapy.* 1988. **62**(12): p. 2507-2516.
9. Kelsey, J.L.J.E.R., *Breast cancer epidemiology: summary and future directions.* 1993. **15**(1): p. 256-63.

10. Bousquenaud, M., et al., *Obesity promotes the expansion of metastasis-initiating cells in breast cancer.* 2018. **20**(1): p. 104.

11. Ahima, R.S., J.S.J.T.i.E. Flier, and Metabolism, *Adipose tissue as an endocrine organ.* 2000. **11**(8): p. 327-332.

12. Kershaw, E.E., J.S.J.T.J.o.C.E. Flier, and Metabolism, *Adipose tissue as an endocrine organ.* 2004. **89**(6): p. 2548-2556.

13. Lakhtakia, R.J.S.Q.U.M.J., *A brief history of breast cancer: Part I: Surgical domination reinvented.* 2014. **14**(2): p. e166.

14. Bradley, C.J., C.W. Given, and C.J.J.o.t.N.C.I. Roberts, *Race, socioeconomic status, and breast cancer treatment and survival.* 2002. **94**(7): p. 490-496.

15. Sung, K.E., et al., *Understanding the impact of 2D and 3D fibroblast cultures on in vitro breast cancer models.* 2013. **8**(10): p. e76373.

16. Weigelt, B., C.M. Ghajar, and M.J.J.A.d.d.r. Bissell, *The need for complex 3D culture models to unravel novel pathways and identify accurate biomarkers in breast cancer.* 2014. **69**: p. 42-51.

17. Murphy, S.V. and A.J.N.b. Atala, *3D bioprinting of tissues and organs.* 2014. **32**(8): p. 773.

18. Zhang, X., Y.J.C.b. Zhang, and biophysics, *Tissue engineering applications of three-dimensional bioprinting.* 2015. **72**(3): p. 777-782.

19. Pusch, K., T.J. Hinton, and A.W.J.H. Feinberg, *Large volume syringe pump extruder for desktop 3D printers.* 2018. **3**: p. 49-61.

20. *Breast Anatomy* National Breast Cancer Foundation 2016.

21. Vacanti, J.P., et al., *Breast tissue engineering*. 1998, Google Patents.

22. Sriraman, N.K.J.C.p.i.p. and a.h. care, *The nuts and bolts of breastfeeding: Anatomy and physiology of lactation.* 2017. **47**(12): p. 305-310.

23. Sarhadi, N., et al., *An anatomical study of the nerve supply of the breast, including the nipple and areola.* 1996. **49**(3): p. 156-164.

24. Segaloff, A.J.R.p.i.h.r., *Hormones and breast cancer.* 2013. **22**: p. 351-379.

25. Harris, H.R., et al., *Body size across the life course, mammographic density, and risk of breast cancer.* 2011. **174**(8): p. 909-918.

26. Gunther, M.J.C.M.A.J., *Lactation in women.* 1942. **47**(5): p. 410.

27. Hankinson, S.E., et al., *Plasma sex steroid hormone levels and risk of breast cancer in postmenopausal women.* 1998. **90**(17): p. 1292-1299.

28. Weinberg, R.A.J.S.A., *How cancer arises.* 1996. **275**(3): p. 62-70.

29. Li, C., D. Uribe, and J.J.B.j.o.c. Daling, *Clinical characteristics of different histologic types of breast cancer.* 2005. **93**(9): p. 1046.

30. Weigelt, B., F.C. Geyer, and J.S.J.M.o. Reis-Filho, *Histological types of breast cancer: how special are they?* 2010. **4**(3): p. 192-208.

31. O'Shaughnessy, J., et al., *Iniparib plus chemotherapy in metastatic triple-negative breast cancer.* 2011. **364**(3): p. 205-214.

32. *Breast Cancer HER2 Status* American Cancer Society

33. Cleator, S., W. Heller, and R.C.J.T.l.o. Coombes, *Triple-negative breast cancer: therapeutic options.* 2007. **8**(3): p. 235-244.

34. Dent, R., et al., *Triple-negative breast cancer: clinical features and patterns of recurrence.* 2007. **13**(15): p. 4429-4434.

35. Rakha, E.A., et al., *Prognostic markers in triple-negative breast cancer.* 2007. **109**(1): p. 25-32.

36. *Cancer Facts & Figures 2019.* American Cancer Society, 2019.

37. Alitalo, A. and M.J.O. Detmar, *Interaction of tumor cells and lymphatic vessels in cancer progression.* 2012. **31**(42): p. 4499.

38. *Treatment for Stage IV (Metastatic) Breast Cancer* American Cancer Society, 2018.

39. Dirat, B., et al., *Cancer-associated adipocytes exhibit an activated phenotype and contribute to breast cancer invasion.* 2011. **71**(7): p. 2455-2465.

40. Havel, P.J.J.P.o.t.N.S., *Role of adipose tissue in body-weight regulation: mechanisms regulating leptin production and energy balance.* 2000. **59**(3): p. 359-371.

41. Belgodere, J.A., et al., *Engineering breast cancer microenvironments and 3D bioprinting.* 2018. **6**.

42. Hoy, A.J., S. Balaban, and D.N.J.T.i.m.m. Saunders, *Adipocyte–tumor cell metabolic crosstalk in breast cancer.* 2017. **23**(5): p. 381-392.

43. Hoarau-Véchot, J., et al., *Halfway between 2D and animal models: are 3D cultures the ideal tool to study cancer-microenvironment interactions?* 2018. **19**(1): p. 181.

44. Cleary, M.P. and M.E.J.E. Grossmann, *Obesity and breast cancer: the estrogen connection.* 2009. **150**(6): p. 2537-2542.

45. Thomas, H.V., et al., *Endogenous estrogen and postmenopausal breast cancer: a quantitative review.* 1997. **8**(6): p. 922.

46. Hormones, E. and B.C.C.G.J.J.o.t.N.C. Institute, *Endogenous sex hormones and breast cancer in postmenopausal women: reanalysis of nine prospective studies.* 2002. **94**(8): p. 606-616.

47. Stephenson, G.D., D.P.J.N. Rose, and cancer, *Breast cancer and obesity: an update.* 2003. **45**(1): p. 1-16.

48. Morimoto, L.M., et al., *Obesity, body size, and risk of postmenopausal breast cancer: the Women's Health Initiative (United States).* 2002. **13**(8): p. 741-751.

49. Rose, D., D. Komninou, and G.J.O.r. Stephenson, *Obesity, adipocytokines, and insulin resistance in breast cancer.* 2004. **5**(3): p. 153-165.

50. Lorincz, A. and S.J.E.-r.c. Sukumar, *Molecular links between obesity and breast cancer.* 2006. **13**(2): p. 279-292.

51. Kim, J.B., et al., *Three-dimensional in vitro tissue culture models of breast cancer—a review.* 2004. **85**(3): p. 281-291.

52. Kapałczyńska, M., et al., *2D and 3D cell cultures–a comparison of different types of cancer cell cultures.* 2018. **14**(4): p. 910.

53. Imamura, Y., et al., *Comparison of 2D-and 3D-culture models as drug-testing platforms in breast cancer.* 2015. **33**(4): p. 1837-1843.

54. Gurski, L.A., et al., *3D matrices for anti-cancer drug testing and development.* 2010. **25**(1): p. 20-25.

55. Kenny, H.A., et al., *Use of a novel 3D culture model to elucidate the role of mesothelial cells, fibroblasts and extra-cellular matrices on adhesion and invasion of ovarian cancer cells to the omentum.* 2007. **121**(7): p. 1463-1472.

56. Martin, K.J., et al., *Prognostic breast cancer signature identified from 3D culture model accurately predicts clinical outcome across independent datasets.* 2008. **3**(8): p. e2994.

57. Weiswald, L.-B., D. Bellet, and V.J.N. Dangles-Marie, *Spherical cancer models in tumor biology.* 2015. **17**(1): p. 1-15.

58. Haycock, J.W., *3D cell culture: a review of current approaches and techniques*, in *3D cell culture*. 2011, Springer. p. 1-15.

59. Haycock, J.W., *3D cell culture*. 2011: Springer.

60. Langhans, S.A.J.F.i.p., *Three-dimensional in vitro cell culture models in drug discovery and drug repositioning.* 2018. **9**: p. 6.

61. Alemany-Ribes, M. and C.E.J.A.d.d.r. Semino, *Bioengineering 3D environments for cancer models.* 2014. **79**: p. 40-49.

62. Dadsetan, M., et al., *Effect of hydrogel porosity on marrow stromal cell phenotypic expression.* 2008. **29**(14): p. 2193-2202.

63. Kolesky, D.B., et al., *3D bioprinting of vascularized, heterogeneous cell-laden tissue constructs.* 2014. **26**(19): p. 3124-3130.

64. Yamada, K.M. and E.J.C. Cukierman, *Modeling tissue morphogenesis and cancer in 3D.* 2007. **130**(4): p. 601-610.

65. Nyga, A., et al., *3D tumour models: novel in vitro approaches to cancer studies.* 2011. **5**(3): p. 239.

66. Sutherland, R.M.J.S., *Cell and environment interactions in tumor microregions: the multicell spheroid model.* 1988. **240**(4849): p. 177-184.

67. Ventola, C.L.J.P. and Therapeutics, *Medical applications for 3D printing: current and projected uses.* 2014. **39**(10): p. 704.

68. Knowlton, S., et al., *Bioprinting for cancer research.* 2015. **33**(9): p. 504-513.

69. Pati, F., J. Gantelius, and H.A.J.A.C.I.E. Svahn, *3D bioprinting of tissue/organ models.* 2016. **55**(15): p. 4650-4665.

70. Asghar, W., et al., *Engineering cancer microenvironments for in vitro 3-D tumor models.* 2015. **18**(10): p. 539-553.

71. Ozbolat, I.T., W. Peng, and V.J.D.d.t. Ozbolat, *Application areas of 3D bioprinting.* 2016. **21**(8): p. 1257-1271.

72. Arslan-Yildiz, A., et al., *Towards artificial tissue models: past, present, and future of 3D bioprinting.* 2016. **8**(1): p. 014103.

73. Zhou, X., et al., *3D bioprinting a cell-laden bone matrix for breast cancer metastasis study.* 2016. **8**(44): p. 30017-30026.

74. King, S.M., S.C. Presnell, and D.G. Nguyen, *Development of 3D bioprinted human breast cancer for in vitro drug screening*. 2014, AACR.

75. Mironov, V., N. Reis, and B.J.T.e. Derby, *Bioprinting: A beginning.* 2006. **12**(4): p. 631-634.

76. Groll, J., et al., *Biofabrication: reappraising the definition of an evolving field.* 2016. **8**(1): p. 013001.

77. Jia, J., et al., *Engineering alginate as bioink for bioprinting.* 2014. **10**(10): p. 4323-4331.

78. Gopinathan, J. and I.J.B.r. Noh, *Recent trends in bioinks for 3D printing.* 2018. **22**(1): p. 11.

79. Zhang, Y.S., et al., *Bioprinting the cancer microenvironment.* 2016. **2**(10): p. 1710-1721.

80. Baker, E.L., et al., *Cancer cell stiffness: integrated roles of three-dimensional matrix stiffness and transforming potential.* 2010. **99**(7): p. 2048-2057.

81. Lee, K.Y. and D.J.J.P.i.p.s. Mooney, *Alginate: properties and biomedical applications.* 2012. **37**(1): p. 106-126.

82. Jang, J., Hee-Gyeong Yi, and Dong Woo Cho., *3D printed tissue models: present and future* ACS Biomaterials Science & Engineering 2016. **2.10**: p. 1722-1731.

83. Hafidz, R.M.R.N., et al., *Chemical and functional propeties of bovine and porcine skin gelatin.* International Food Research Jounral 2011. **18**: p. 813-817.

84. Aronson, J.K., *Side Effects of Drugs Annual: A world-wide yearly survey of new data and trends in adverse drug reactions*. Vol. 26. 2003: Elsevier.

85. Dang, J.M., and Kam W. Leong., *Natural polymers for gene delivery and tissue engineering* Advanced drug delivery reviews, 2006. **58**: p. 487-499.

86. Rutz, A.L., et al, *A multimaterial bioink method for 3D printing tubable, cell-compatible hydrogels.* Advanced Materials 2015. **27**(9): p. 1607-1614.

87. DeSantis, C., et al., *Breast cancer statistics, 2011.* 2011. **61**(6): p. 408-418.

88. Siegel, R., D. Naishadham, and A.J.C.a.c.j.f.c. Jemal, *Cancer statistics, 2013.* 2013. **63**(1): p. 11-30.

89. Siegel, R.L., K.D. Miller, and A.J.C.a.c.j.f.c. Jemal, *Cancer statistics, 2019.* 2019. **69**(1): p. 7-34.

90. Vandeweyer, E. and D.J.A.o.A.-A.A. Hertens, *Quantification of glands and fat in breast tissue: an experimental determination.* 2002. **184**(2): p. 181-184.

91. Tibbitt, M.W., K.S.J.B. Anseth, and bioengineering, *Hydrogels as extracellular matrix mimics for 3D cell culture.* 2009. **103**(4): p. 655-663.

92. Bougaret, L., et al., *Adipocyte/breast cancer cell crosstalk in obesity interferes with the anti-proliferative efficacy of tamoxifen.* 2018. **13**(2): p. e0191571.

93. Reeves, G.K., et al., *Cancer incidence and mortality in relation to body mass index in the Million Women Study: cohort study.* 2007. **335**(7630): p. 1134.

94. Celis, J.E., et al., *Identification of extracellular and intracellular signaling components of the mammary adipose tissue and its interstitial fluid in high risk breast cancer patients: toward dissecting the molecular circuitry of epithelial-adipocyte stromal cell interactions.* 2005. **4**(4): p. 492-522.

95. Perera, C.N., et al., *Identification of proteins secreted from leptin stimulated MCF-7 breast cancer cells: a dual proteomic approach.* 2008. **233**(6): p. 708-720.

96. Duong, M.N., et al., *The fat and the bad: Mature adipocytes, key actors in tumor progression and resistance.* 2017. **8**(34): p. 57622.

97. Bochet, L., et al., *Unraveling the obesity and breast cancer links: a role for cancer-associated adipocytes?*, in *Adipose Tissue Development*. 2010, Karger Publishers. p. 45-52.

98. Ling, K., et al., *Bioprinting-based high-throughput fabrication of three-dimensional MCF-7 human breast cancer cellular spheroids.* 2015. **1**(2): p. 269-274.

99. Burg, K.J., D. Dréau, and T. Burg, *Engineering 3D Tissue Test Systems*. 2017: CRC Press.

100. Krouskop, T.A., et al., *Elastic moduli of breast and prostate tissues under compression.* 1998. **20**(4): p. 260-274.

101. McKnight, A.L., et al., *MR elastography of breast cancer: preliminary results.* 2002. **178**(6): p. 1411-1417.

102. Sarvazyan, A.P., et al., *Shear wave elasticity imaging: a new ultrasonic technology of medical diagnostics.* 1998. **24**(9): p. 1419-1435.

103. Chang, J.M., et al., *Stiffness of tumours measured by shear-wave elastography correlated with subtypes of breast cancer.* 2013. **23**(9): p. 2450-2458.

104. Stanton, M., J. Samitier, and S.J.L.o.a.C. Sanchez, *Bioprinting of 3D hydrogels.* 2015. **15**(15): p. 3111-3115.

105. Kong, H.J., E. Wong, and D.J. Mooney, *Independent Control of Rigidity and Toughness of Polymeric Hydrogels*. 2003, ACS AMERICAN CHEMICAL SOCIETY: United States. p. 4582.

106. Shengmao, L. and G. Linxia, *Influence of Crosslink Density and Stiffness on Mechanical Properties of Type I Collagen Gel.* Materials, 2015(2): p. 551.

107. Galic, S., et al., *Adipose tissue as an endocrine organ.* 2010. **316**(2): p. 129-139.

108. Berry, R., et al., *Adipose Tissue-Residing Progenitors (Adipocyte Lineage Progenitors and Adipose-Derived Stem Cells (ADSC)).* 2015. **1**(3): p. 101-109.

109. Deng, Z., et al., *Dedifferentiation of mature adipocytes with periodic exposure to cold.* 2019(Preprint): p. 1-10.

110. Petan, T., E. Jarc, and M.J.M. Jusović, *Lipid droplets in cancer: guardians of fat in a stressful world.* 2018. **23**(8): p. 1941.

111. Xu, F., et al., *A three-dimensional in vitro ovarian cancer coculture model using a high-throughput cell patterning platform.* 2011. **6**(2): p. 204-212.

112. Hockel, M. and P.J.J.o.t.N.C.I. Vaupel, *Tumor hypoxia: definitions and current clinical, biologic, and molecular aspects.* 2001. **93**(4): p. 266-276.

113. Prentice, A.M.J.I.j.o.e., *The emerging epidemic of obesity in developing countries.* 2005. **35**(1): p. 93-99.

114. Kishimoto, T. and T.J.E.o.I.D. Tanaka, *Interleukin 6.* 2015: p. 1-8.

115. Kern, P.A., et al., *Adipose tissue tumor necrosis factor and interleukin-6 expression in human obesity and insulin resistance.* 2001. **280**(5): p. E745-E751.

116. Blaber, S.P., et al., *Analysis of in vitro secretion profiles from adipose-derived cell populations.* 2012. **10**(1): p. 172.

117. Schäffler, A. and C.J.S.c. Büchler, *Concise review: adipose tissue‐derived stromal cells—basic and clinical implications for novel cell‐based therapies.* 2007. **25**(4): p. 818-827.

118. Pittenger, M.F., et al., *Multilineage potential of adult human mesenchymal stem cells.* 1999. **284**(5411): p. 143-147.

119. Dicker, A., et al., *Functional studies of mesenchymal stem cells derived from adult human adipose tissue.* 2005. **308**(2): p. 283-290.

120. Myers Jr, M.G., et al, *Obesity and leptin resitance: distinguishing cause from effect* Trends in Endocrinology & Metabolism 2010. **21**(11): p. 643-651.

121. Ravussin, E., *Adiponectin enhances insulin action by decreasing ectopic fat deposition*. 2002, Nature Publishing Group.

122. Hu, E., P. Liang, and B.M.J.J.o.b.c. Spiegelman, *AdipoQ is a novel adipose-specific gene dysregulated in obesity.* 1996. **271**(18): p. 10697-10703.

123. Yamauchi, T., et al., *The fat-derived hormone adiponectin reverses insulin resistance associated with both lipoatrophy and obesity.* 2001. **7**(8): p. 941.

124. Arita, Y., et al., *Paradoxical decrease of an adipose-specific protein, adiponectin, in obesity.* 1999. **257**(1): p. 79-83.

125. Mantzoros, C., et al., *Adiponectin and breast cancer risk.* 2004. **89**(3): p. 1102-1107.

126. Miyoshi, Y., et al., *Association of serum adiponectin levels with breast cancer risk.* 2003. **9**(15): p. 5699-5704.

127. Jardé, T., et al., *Molecular mechanisms of leptin and adiponectin in breast cancer.* 2011. **47**(1): p. 33-43.

128. Grossmann, M., et al., *Effects of adiponectin on breast cancer cell growth and signaling.* 2008. **98**(2): p. 370.

129. Körner, A., et al., *Total and high-molecular-weight adiponectin in breast cancer: in vitro and in vivo studies.* 2007. **92**(3): p. 1041-1048.

130. Christian, S.L., et al., *Collagen overlays can inhibit leptin and adiponectin secretion but not lipid accumulation in adipocytes.* 2018. **6**: p. e4641.